

# The South Patagonian batholith: 150 my of granite magmatism on a plate margin

F. Hervé<sup>a,\*</sup>, R.J. Pankhurst<sup>b</sup>, C.M. Fanning<sup>c</sup>, M. Calderón<sup>a</sup>, G.M. Yaxley<sup>c</sup>

<sup>a</sup> *Departamento de Geología, Universidad de Chile, Casilla 13518, Correo 21, Santiago, Chile*

<sup>b</sup> *NERC Isotope Geosciences Laboratory, Keyworth, Nottingham NG12 5GG, UK*

<sup>c</sup> *PRISE, Research School of Earth Sciences, The Australian National University, Mills Road, Canberra ACT 0200, Australia*

Received 7 June 2006; accepted 26 January 2007

Available online 1 February 2007

## Abstract

A new database of 70 U–Pb zircon ages (mostly determined by SHRIMP) indicates that the South Patagonian batholith resulted from the amalgamation of subduction-related plutons from the Late Jurassic to the Neogene. Construction of the batholith began with a voluminous, previously undetected, Late Jurassic bimodal body mainly composed of leucogranite with some gabbro, emplaced along its present eastern margin within a restricted time span (157 to 145 Ma). This episode is, at least in part, coeval with voluminous rhyolitic ignimbrites of the Tobifera Formation, deposited in the deep Rocas Verdes Basin east of the batholith; this was the last of several southwestward-migrating silicic volcanic episodes in Patagonia that commenced in an Early Jurassic extensional tectonic regime. The quasi-oceanic mafic floor of the basin was also contemporaneous with this Late Jurassic batholithic event, as indicated by mutually cross-cutting field relationships. Changes in subduction parameters then triggered the generation of earliest Cretaceous plutons (Cretaceous 1: 144–137 Ma) west of the Late Jurassic ones, a westward shift that culminated at 136–127 Ma (Cretaceous 2) along the present western margin of the batholith. Most mid- to Late Cretaceous (Cretaceous 3: 126–75 Ma) and Paleogene (67–40 Ma) granitoids are represented by geographically restricted plutons, mainly emplaced between the previously established margins of the batholith, and mostly in the far south; no associated volcanic rocks of similar age are known at present in this area. During the final Neogene stage of plutonism (25–15 Ma) a recurrence of coeval volcanism is recognized within and east of the batholith. Typical  $\epsilon\text{Ndt}$  values for the granitoids vary from strongly negative (–5) in the Late Jurassic, to progressively higher values for Cretaceous 1 (–4), Cretaceous 2 (–0.7), Cretaceous 3 (+2) and the Paleogene (+5), followed by lower and more variable ones in the Neogene (–1 to +5). These variations may reflect different modes of pluton emplacement: large crustal magma chambers developed in the early stages (Late Jurassic to Cretaceous 1), leading to widespread emplacement of plutons with a crustal signature, whereas the Cretaceous 2, Cretaceous 3 and Palaeogene parts of the batholith resulted from incremental assembly of small plutons generated at greater depths and with higher  $\epsilon\text{Ndt}$ . This does not in itself justify the idea of a reduction in crustal character due to progressive exhaustion of fusible material in the crust through which the magmas passed. © 2007 Elsevier B.V. All rights reserved.

**Keywords:** Batholith; Mesozoic–Cenozoic; Patagonia; SHRIMP U–Pb ages

## 1. Introduction

Cordilleran batholiths, notably those along the western coasts of the Americas, are a characteristic product of subduction processes on active continental

\* Corresponding author.

*E-mail addresses:* [fherv@cec.uchile.cl](mailto:fherv@cec.uchile.cl) (F. Hervé), [rjpt@bas.ac.uk](mailto:rjpt@bas.ac.uk) (R.J. Pankhurst), [Mark.Fanning@anu.edu.au](mailto:Mark.Fanning@anu.edu.au) (C.M. Fanning).

margins. As we demonstrate here, they may represent magmatic activity over 100 m.y. or more on the same general axis with respect to the continental margin, and thus their study is critical to understanding the nature and development of subduction parameters through time. Accurate and precise dating of the igneous rocks is needed in order to define their distribution, sequence of emplacement, and relationship to external events. However, because long-term magmatism in a single location can lead to complex resetting of K–Ar and Rb–Sr geochronological systems, we base this study on the premise that U–Pb zircon dating is the most robust basis for establishing a reliable chronological framework. Field and geochemical studies in composite batholiths such as these also lead to better understanding of magma genesis and modes of emplacement of plutonic bodies.

In this paper we present the main results of a six year project investigating the granitoid rocks of the South Patagonian batholith (SPB). These include a database of 70 U–Pb zircon ages for crystallization, together with 51 new geochemical analyses of major trace and REE elements, and 41 Nd–Sr isotopic determinations. Based on these data, and those from previous studies of the SPB (see below), the age structure is revealed and some aspects of the emplacement and genesis of the batholith are addressed.

## 2. Tectonic setting

The SPB is part of the huge Mesozoic to Cenozoic Patagonian batholith (Fig. 1), which extends continuously along the Andean continental margin of South America between the latitudes 40°S and 56°S. The batholith is usually subdivided into three segments: the North Patagonian batholith (NPB) north of 47°S (the approximate latitude of the Chile Triple Junction), the South Patagonian batholith (47–53°S), and the Fuegian batholith, which extends to the extreme southern end of the continent. The North Patagonian batholith was largely developed by eastward subduction of the Nazca plate, whereas the Fuegian batholith developed over the present-day Scotia microplate. The SPB is located where at present the Antarctic plate is being subducted beneath South America, but this tectonic configuration was only established in the late Cenozoic, as the triple junction migrated northwards from the southern tip of the continent after about 15 Ma; most, if not all, of the batholith was generated before this time.

The earliest indication that subduction processes were active in the area is the accretion of the Madre de Dios exotic terrane, at some time between the Middle Permian and the earliest Jurassic. The accretion of this

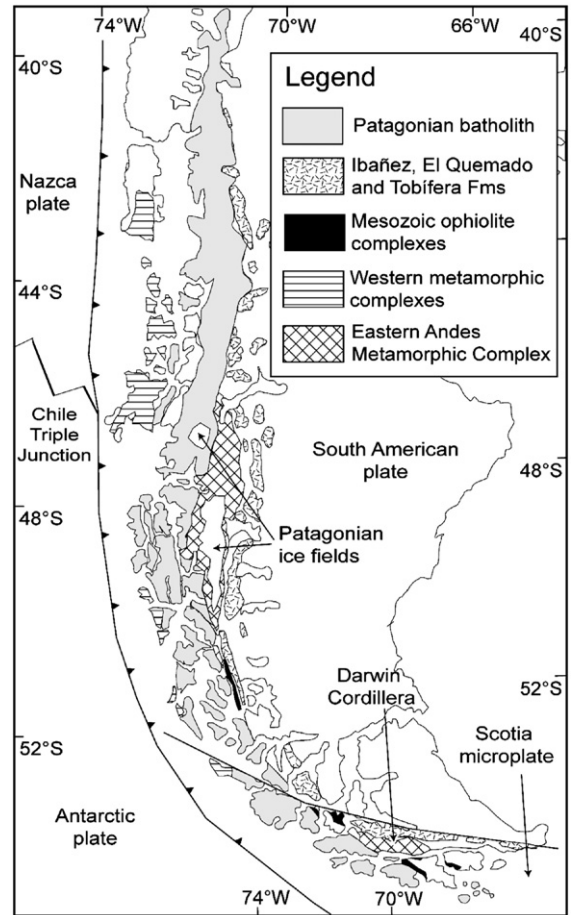


Fig. 1. Location map of the South Patagonian batholith (SPB) in the Patagonian Andes. Also indicated are the late Paleozoic to early Mesozoic metamorphic complexes into which the SPB is intruded, the Mesozoic ophiolitic complexes which formed in the Rocas Verdes basin including the northernmost Sarmiento complex, and the mainly silicic volcanic Late Jurassic Tobifera Formation.

exotic block took place from the northwest (Rapalini et al., 2001), suggesting that subduction was highly oblique to the continental margin. This may explain the fact that no plutonic rocks assigned to that age interval are found within the batholith: alternatively, flat subduction could have displaced magmatic activity farther to the east, beyond the present margins of the exposed batholith. Rapela et al. (2005) report Early Jurassic Cordilleran style granite magmatism on the eastern side of the Andes between 41° and 45°S (i.e., at the latitude of the NPB), in a belt trending NNW–SSE, indicating an earlier phase of subduction coeval with the Karoo mantle plume at  $182 \pm 2$  Ma. At the same time, eastern and central Patagonia were covered by thick rhyolite ignimbrite flows, generated, at least initially, by deep crustal melting in response to the spreading plume-head;

as volcanism migrated westwards, it developed a more arc-like character (Gust et al., 1985; Féraud et al., 1999; Pankhurst et al., 2000; Riley et al., 2001).

The crust into which the batholith was emplaced underwent regional extension during the late-Middle to early-Late Jurassic, accompanied by voluminous bimodal volcanism (mainly rhyolitic) representing the last stage of the ignimbrite episode described above, to about 154 Ma — the El Quemado and Ibáñez formations in the north and Tobífera Formation in the south (Bruhn et al., 1978; the V3 volcanic group of Pankhurst et al., 2000). Early two-mica granite plutons coeval with this volcanism have been recognized beyond the margins of the batholith in Cordillera Darwin, Tierra del Fuego ( $164.1 \pm 1.7$  Ma; Mukasa and Dalziel, 1996) and the Diego de Almagro archipelago ( $\sim 170$  Ma; Hervé and Fanning, 2003). Hornblende and biotite granitoids have been dated at  $\sim 155$  Ma in satellite plutons east of the main margin of the batholith farther north (Parada et al., 1997; Pankhurst et al., 2000), but until the present study the oldest confirmed age of plutonism within the main part of the batholith was a single U–Pb zircon age of  $149.6 \pm 0.8$  Ma from the head of Fiordo Baker (Bruce et al., 1991).

According to presently accepted ideas, in latest Jurassic and Early Cretaceous times, the SPB magmatic arc became separated from the continent by a developing marginal basin (the Rocas Verdes basin) floored by quasi-oceanic crust. This basin was widest in the south, but was progressively narrower northwards as far as  $51^\circ\text{S}$ , beyond which it did not develop (Katz, 1964; Dalziel and Cortés, 1972). The marginal basin closed again by the Late Cretaceous (Bruhn and Dalziel, 1977). The Diego de Almagro complex is the only unit where blueschists generated in the subduction zone are exposed (Willner et al., 2004); these rocks were subducted, metamorphosed, deformed and exhumed through the Cretaceous in a shear zone setting with a large component of subhorizontal sinistral shearing (Olivares et al., 2003), again suggesting oblique subduction from the northwest.

Subduction was probably continuous after the inception of the SPB in the Late Jurassic but the subduction parameters of the Nazca plate changed with time (Pardo-Casas and Molnar, 1987; Somoza, 1998), at least during the Cenozoic. The subduction direction varied from sub-parallel to the continental margin in the earliest Cenozoic, progressively rotating to northwesterly-directed subduction until the Miocene, when it became almost perpendicular to the continental margin, and with a similar direction to present-day subduction north of the Chile triple junction. The rate of subduction also varied

through time, and in the North Patagonian batholith Pankhurst et al. (1999) showed that there is a relationship between raised subduction velocities and plutonic episodes during the Cenozoic.

### 3. Previous research

An early geochemical study of the SPB is that of Stern and Stroup (1982), but the most comprehensive previous work is that of Weaver et al. (1990) and Bruce et al. (1991), who conducted petrological, geochemical and geochronological investigations on three main transects across the batholith. They summarized earlier geochronological data from Halpern (1973), Hervé et al. (1981, 1984), Suárez et al. (1986, 1987) and Weaver et al. (1990) together with their own results. This database is dominated by K–Ar ages (43) and Ar–Ar ages (41), with a few Rb–Sr whole-rock or whole rock–mineral isochrons (6) and conventional multigrain U–Pb zircon ages (4). Bruce et al. (1991) concluded that magmatism in the SPB resulted in the generation of lithologies ranging from gabbro to granite over the period 165 to 11 Ma, with a peak between 120 and 70 Ma. However, the older end of this range was entirely based on dating of the Darwin Cordillera two-mica granite in the Fuegian batholith ( $157 \pm 8$  Ma, Rb–Sr whole-rock isochron, Hervé et al., 1981). They suggested that within restricted areas of the batholith plutonism appears episodic and diachronous with adjacent areas. Each area exhibits a change from gabbro to granite over tens of millions of years, accompanied by a decrease in initial  $^{87}\text{Sr}/^{86}\text{Sr}$  ratios. This was interpreted via a model in which the older plutons generally intruded country rocks on the margins of the batholith, whereas the younger plutons occur near the central axis of the batholith, where they were isolated from contamination with the radiogenic country rocks in a manner that became increasingly efficient through time. They remarked on the general lack of deformed plutons, which they took as an indication of a neutral to extensional state of stress at mid-crustal levels during the episodes of pluton emplacement.

Martin et al. (2001) presented 7 new conventional U–Pb zircon ages from around latitude  $48^\circ\text{S}$ , and Fanning et al. (2001) and Hervé et al. (2003) mention 8 additional U–Pb SHRIMP zircon ages. These results are incorporated with 45 further U–Pb SHRIMP zircon ages obtained in this study, to form an extended U–Pb zircon age database for the SPB.

Thomson et al. (2001) remarked that zircon FT ages from the SPB reflect cooling to shallow crustal levels shortly after intrusion, and that apatite FT ages record accelerated cooling and denudation at ca. 30 Ma, with

maximum denudation rates migrating from west to east to the present-day Andean topographic divide. However, Massonne et al. (2004) present thermobarometric evidence that two-mica granites in the eastern border of the batholith crystallised at depths of 20 km or more.

**4. Field aspects**

Our fieldwork was carried out over five annual seasons, working from small boats. From several hundred miles of coastal exposure observed, 472 outcrops were visited and sampled, and 245 samples were studied in thin section. Nevertheless, in view of the huge size of the batholith, this probably still represents no more than a detailed reconnaissance examination. Most of the studied outcrops are near the shoreline, where surfaces scoured by glaciers give outcrops where

fresh rocks may sometimes be observed and sampled. However, continuity of accessible outcrop is restricted, with hiatuses represented by the maze of open waterways (up to half the surface area), so that observation of contacts between different plutonic phases in the field is a rare and serendipitous occurrence. Screens of country rocks within the batholith are rare, and tend to occur only near the margins.

The eastern contact of the SPB is generally against regionally metamorphosed Palaeozoic psammopelitic rocks of the basement complexes; on the whole it is easily defined and accessible at the heads of the eastern fjords (some of which are very long). The exception is in the Cordillera Sarmiento region, where it is in contact with ophiolites of the Rocas Verdes basin. On the other hand, the western margin can only locally be observed (Fig. 2) since the SPB commonly extends to the

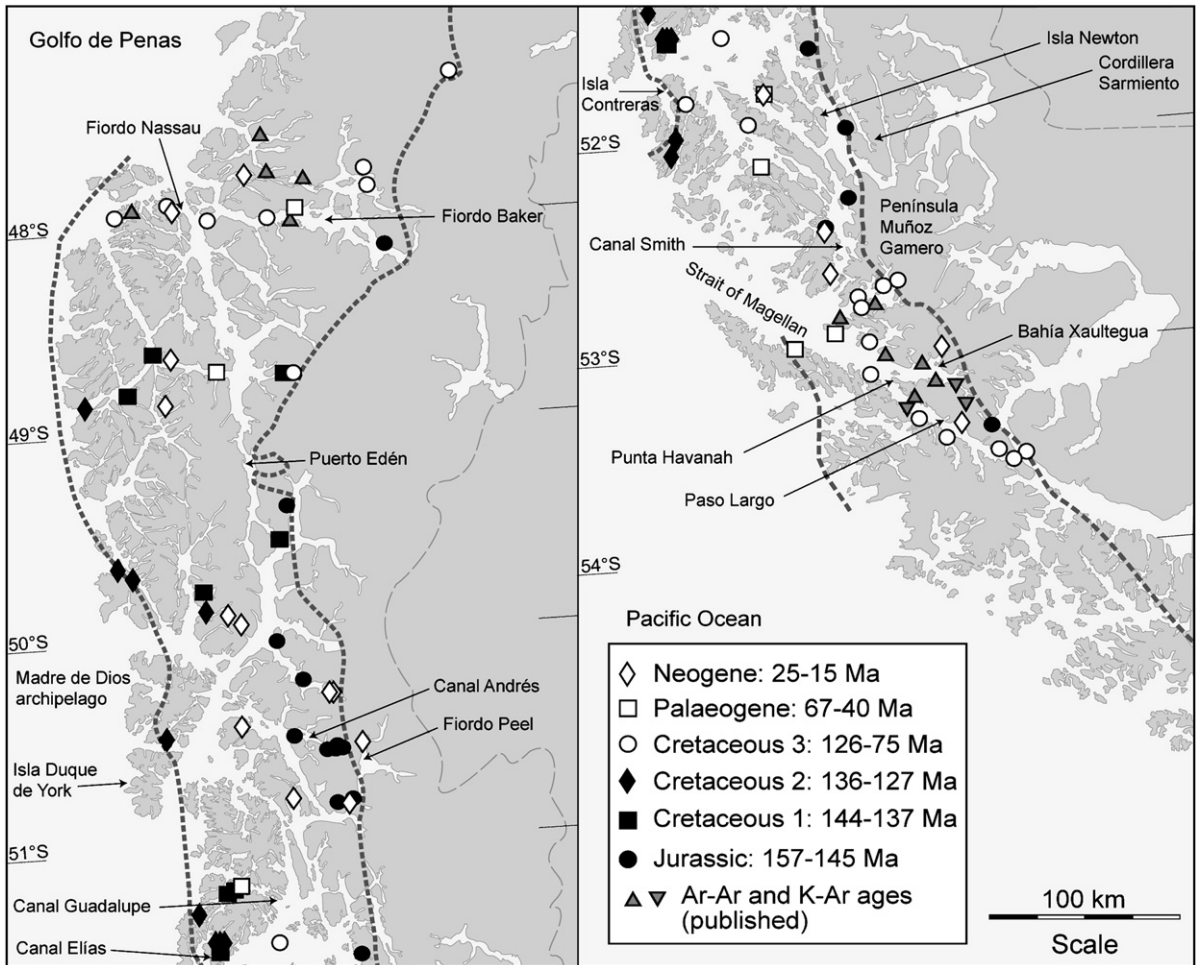


Fig. 2. Sketch map showing the distribution of the U–Pb SHRIMP zircon age categories as described in text. For actual ages, see Table 1 and Electronic annex EA-1. Location of Ar–Ar and K–Ar ages after Weaver et al. (1990) and Bruce et al. (1991).

westernmost limit of the archipelago. The sharp eastern margin often exhibits a metamorphic aureole in the metasedimentary rocks, and Calderón and Hervé (2000) have recognized biotite and andalusite/sillimanite zones on approaching the contact. At Punta Havanah, decametre-scale subhorizontal bodies of leucocratic granite intrude the basement rocks. In some sectors, the contact has been described as faulted (Harambour, 2002). The western margin of the SPB is observed in the Madre de Dios Archipelago and on Isla Contreras, where contact metamorphic effects seem to be less intense than at the eastern contact. On Isla Contreras, the granitic body has a gently east-dipping concordant contact with a foliated biotite hornfels to the west.

Internal contacts between plutonic bodies have been observed in some areas. Steeply inclined contacts between gabbro and leucogranite are observable in a number of places close to the western margin, for example in Canal Guadalupe, where they can be clearly seen on barren slopes for some kilometres. On Isla Newton, leucogranite cuts gabbro. A succession of decametre-scale vertical bodies of different lithologies can be observed at Canal Elías and in the northern shore of Paso Largo, Strait of Magellan. However, it has been impossible to delimit any individual pluton by continuous observation of such contacts. Observation of areas with homogeneous lithologies suggests that individual plutons are usually 1 to 10 km in horizontal dimension. Exceptions are metre-scale mafic dykes that are present in most outcrops, and which account for up to 50% in volumetric abundance in some exposures. Dykes are usually sub-vertical, but in Fiordo Baker a granitic body also shows a set of subhorizontal mafic dykes, cross-cutting the vertical ones. At Canal Smith, dyke-free granite cuts across a tonalite with 30% dykes, an indication that dykes are not necessarily younger than the overall plutonic activity. Mafic enclaves are a common feature in many outcrops, although leucogranites appear to be devoid of this feature. At Canal Elías, mafic inclusions and tonalitic–granodioritic host rocks are largely coeval, as are cross-cutting leucogranites.

The observed predominance of vertical contacts between plutons suggests vertical dyke-like emplacement of the plutons. Mid-crustal levels are suggested by the mineralogy of the eastern contact aureole and Al-in-Hbl thermobarometry in some plutons (Calderón, 2000; Dzogolyk et al., 2003; Massonne et al., 2004; Calderón, 2005). Magmatic foliation is not uncommon in the plutons, which more rarely show well defined igneous layering. Ductile and brittle shear zones occur sparsely, and they are better observed where dykes are present. Their study and significance is beyond the scope of this paper.

## 5. Analytical methods

### 5.1. SHRIMP

The new U–Pb SHRIMP ages determined for this investigation were obtained on zircon concentrates prepared in the Departamento de Geología, Universidad de Chile, using SHRIMP II at RSES, ANU, Canberra. The measurement techniques employed followed those of Williams (1998), except that for 34 samples only ~8 different areas were measured in order to obtain ages for a more representative number of samples; these data mostly resulted in satisfactory ages and derived errors, albeit often based on only 5–6 data points (Table 1; supplementary data in Electronic annex EA-1). FC1 was used as the standard throughout, and the data were processed using SQUID and Isoplot/EX (Ludwig, 1999). The new results, together with the most reliable published data for crystallization age of the plutonic rocks, are plotted in Fig. 2, and some representative age probability plots for individual samples in Fig. 3.

### 5.2. XRFs and ICP-MS

Samples were pulverised in an agate ring-mill. Major and minor element whole rock geochemical analyses were obtained by X-ray Fluorescence Spectroscopy at Geoscience Australia, Canberra, on glass fusion discs prepared with a borate flux in the mass ratio 9:1.

Trace elements were measured at The Australian National University by laser-ablation ICP-MS, (a simple, rapid and cost-effective technique) on new glass beads prepared using high purity lithium metaborate flux (Sigma Chemicals, Analytical Grade). Flux/sample mixtures (in the approximate ratio 2:1) were loaded in newly prepared graphite crucibles and fused at 1200 °C in an Ar atmosphere in a box furnace, and then quenched to glass in water. The beads were mounted in 1 in. epoxy mounts, examined under a reflected light microscope to ensure that they were completely aphyric, and polished. As well as 51 SPB samples, three duplicates and secondary standards AGV-2, BCR2g, BIR-1 and AC-E (Govindaraju, 1994) were prepared in the way described above. LA-ICP-MS analysis used an Excimer UV laser (193 nm), a custom built sample introduction system (Eggins et al., 1998a) and a Hewlett-Packard Agilent 7500 quadrupole mass spectrometer. The spot size was 142 µm, and the laser was pulsed at 5 Hz, delivering 100 mJ per pulse.

Ablation was conducted under a mixed He+H<sup>2</sup> atmosphere and the ablated material was carried to the plasma in an Ar/He gas stream. The instrument was

Table 1  
Summary of U–Pb zircon ages

Sample	Rock type	Locality	Lat.	Long.	N°of spots	MSWD	Age	95% c.l.	Method	
FO0345a	Gabbro	Puerto Henry	53°25.23'	72°35.63'	6 of 8	1.70	156.9	3	SHRIMP	For 6 of 8, 1 significantly older ~340 Ma, and 1 with radiogenic Pb loss
FO0412	Dacite	Estero Andres	50°32.74'	73°51.91'	5 of 12	1.15	156.5	2	SHRIMP	Bimodal age distribution, with some radiogenic Pb loss and some older areas. Major age is 156.5 Ma
FO0415	Granodiorite	Seno Andrés	50°32.11'	73°53.80'	6 of 8	0.65	155.5	2	SHRIMP	Some radiogenic Pb loss
ST0340a	Granite	Seno Profundo	51°55.77'	73°36.20'	7 of 8	0.99	154.5	2	SHRIMP	Minor radiogenic Pb loss, dominantly simple age otherwise
FO0015	Massive Rhyolite	Fiordo Peel	50°32.411'	73°43.156	11 of 15	1.40	152.0	2	SHRIMP	Some radiogenic Pb loss
FO00105	Granite	Pen Staines	51°31.98'	73°48.84'	5 of 9	0.64	152.0	2	SHRIMP	For 5 of 9, others with high U are older $\geq$ ~156 Ma
FO0410	Granodiorite	Puerto Polcos	50°31.92'	73°56.73'	8 of 8	1.00	151.0	1	SHRIMP	Simple magmatic age
FO0009	Foliated Granite	Fiordo Peel	50°40.13'	73°46.48'	11 of 16	1.19	150.1	1	SHRIMP	Triassic inheritance, dominant age group with subordinate older group at c.155 Ma
FF9909B	Granodiorite	Fiordo Eyre	49°21.39'	74°06.39'	13 of 19	1.70	149.9	2	SHRIMP	Some Permian cores analysed, some radiogenic Pb loss and a diffuse age distribution for the magmatic "age"
SE9811	Granite	Seno Europa	49°59.815'	74°20.056'	10 of 18	2.00	149.6	2	SHRIMP	Some inheritance, and some radiogenic Pb loss, dispersed "magmatic" age grouping
FO0004	Granite	Fiordo Peel	50°47.89'	73°54.21'	15 of 16	1.30	149.5	1	SHRIMP	Minor radiogenic Pb loss
FO0054	Granite	Peninsula Muñoz G	52°15.37'	73°35.38'	12 of 15	1.50	149.3	1	SHRIMP	Some inheritance at ~155 Ma
FO0407a	Granite	Seno Andres	50°27.87'	74°10.96'	7 of 8	0.65	148.8	2	SHRIMP	1 slightly older analysis
FO0416	Diorite	Seno Andrés	50°33.46'	73°52.62'	3 of 8	0.28	148.8	2	SHRIMP	Wide range in U and ages, some Jurassic and older. Lower U and young age group given
FO0327a	Granodiorite	Canal Bambach	52°25.50'	73°44.98'	5 of 6	1.30	148.3	3	SHRIMP	For 5 of 6 analyses — 1 significantly older with ~2800 ppm U — ~155 Ma
FO0328a	Gabbro	Canal Bambach	52°24.66'	73°44.62'	6 of 10	0.47	147.8	2	SHRIMP	For 6 analyses, 2 older ~153 Ma, 1 at ~100 Ma and one with radiogenic Pb loss
SE9806	Tonalite	Seno Europa	50°11.90'	74°09.90'	17 of 21	1.17	145.0	1	SHRIMP	One Pan African and one Grenville analysis, two with radiogenic Pb loss leaving a dominantly simple age
FO0035	Granite	Canal Elias	51°27.97'	74°52.02'	8 of 9	1.02	144.2	1	SHRIMP	For 8 of 9, 1 enriched in common Pb and has lost radiogenic Pb
FO0037	Granite	Estero Benjamin	51°13.144'	74°47.441'	8 of 8	1.08	142.8	1	SHRIMP	Simple magmatic age
SI9926	Tonalite	Seno Iceberg	48°43.72'	74°01.19'	9 of 12	0.43	142.5	1	SHRIMP	
IW9807a	Granite	Seno Stange	49°45.17'	74°45.31	18 of 20	1.02	141.6	1	SHRIMP	One very young analysis high in common Pb; dominantly simple age population at 142 Ma
FO0038	Granodiorite	Estero Benjamin	51°11.38'	74°44.00'	9 of 19	1.10	140.7	1	SHRIMP	Bimodal age distribution, the more prominent grouping is at 145 Ma
FF99-10C	Granite	Fiordo Eyre	49°32.05'	74°11.08'			140.2	0.2	TIMS	<a href="#">Martin et al. (2001)</a>
FO0030	Granodiorite	Canal Elías	51°26.665'	74°53.048'	14 of 18	1.18	139.9	1	SHRIMP	Some radiogenic Pb loss and some inheritance
FO0031	Gabbro–diorite	Canal Elías	51°27.647'	74°52.872'	14 of 18	0.57	139.5	1	SHRIMP	Inheritance at 145–150 Ma
CC9920	Granodiorite	Canal Cochran	48°46.03'	75°11.86'	8 of 10	0.34	138.8	1	SHRIMP	
CA99-16A	Granodiorite	Canal Fallos	48°34.61'	74°57.29'			137.8	0.2	TIMS	<a href="#">Martin et al. (2001)</a>
EC99-18	Granodiorite	Estrecho Castillo	48°48.15'	75°27.96'			136.1	0.2	TIMS	<a href="#">Martin et al. (2001)</a>
FO0087	Gabbro	Canal Nogueira	51°57.27'	74°50.31'	5 of 9	0.79	135.9	2	SHRIMP	For 5 of 9 analyses, 3 older $\geq$ ~140 Ma
IW9821	Granite–cataclasite	Canal Picton	49°42.46'	75°14.97'	10 of 12	0.81	135.6	1	SHRIMP	
FO0029	Tonalite	Canal Elías	51°26.665'	74°53.048'	14 of 15	1.50	134.4	2	SHRIMP	Minor radiogenic Pb loss
FO0420	Granite	Isla Caraciolo	50°27.60'	75°07.81'	8 of 8	1.08	132.7	1	SHRIMP	Simple magmatic age
FO0089	Granodiorite	Canal Nogueira	52°00.51'	74°55.26'	4 of 6	2.60	130.0	6	SHRIMP	For 4 of 6, significant scatter overall, other 2 are younger with ?Pb loss
FO0036	Granodiorite	Estero Benjamin	51°19.273'	74°58.567'	8 of 9	1.06	128.2	2	SHRIMP	For 8 of 9: 1 with ?radiogenic Pb loss
IW9811	Granite	Seno Marsh	49°50.96'	74°48.19'	17 of 20	1.08	127.7	1	SHRIMP	3 slightly older grains at ~133 Ma, others form simple population
IW9819	Diorite	Paso Escarceo	49°35.60'	75°22.19'	15 of 21	0.56	126.7	1	SHRIMP	Skewed distribution due to slightly older group at ~130 Ma
FO0218a	Tonalite	Canal Irene	52°43.59'	73°22.07'	14 of 19	1.08	126.3	1	SHRIMP	Some dispersion about the major peak; 2 slightly older, 3 with radiogenic Pb loss
SI99-25	Granodiorite	Seno Iceberg	48°43.62'	73°59.40'			121.9	0	TIMS	<a href="#">Martin et al. (2001)</a>
FO98P14	Tonalite	Fiordo Larena	47°58.18'	74°18.81'			ca 120		SHRIMP	

FO0094	Diorite	Canal Nogueira	51°28.79'	74°31.14'	12 of 12	1.30	119.2	2	SHRIMP	
THC14	Granodiorite	Cochrane	47°35.55'	72°51.09'			118.7	1	TIMS	Martin et al. (2001)
FO98P13	Tonalite	Canal Somerset	47°58.93'	74°35.48'	9 of 10	0.86	116.8	2	SHRIMP	
FO0072b	Gabbro–diorite	Canal Nogueira	51°47.72'	74°46.16'	8	–	–	–	SHRIMP	Significant scatter, 5 cluster about 115 Ma
FO0332	Diorite	Isla Santa Ines	53°25.78'	72°54.76'	5 of 6	0.87	111.3	2	SHRIMP	For 5 of 6 analyses — 1 with radiogenic Pb loss
FO0222b	Diorite	Isla Leucotón	52°45.86'	73°34.07'	13 of 19	0.82	98.9	1	SHRIMP	Some dispersion; a group of “older” analyses ≥ 100 Ma, some radiogenic Pb loss
FO0222a	Diorite	Isla Leucotón	52°45.87'	73°34.07'	11	–	–	–	SHRIMP	Significant scatter, one Proterozoic zircon, two general clusters between ~74–82 Ma and ~90–98 Ma
FO0065	Gabbro–diorite	Canal Cuttler	52°06.49'	73°54.14'	6 of 7	0.66	94.7	2	SHRIMP	For 5 of 6 analyses — 1 older at ~100 Ma
FO0351a	Gabbro	Bahia Barcelo	53°30.56'	72°33.53'	9 of 11	1.20	94.1	2	SHRIMP	For 9 of 11 analyses; two older at about 102 Ma
FO0219a	Granodiorite	Puerto Arturo	52°41.96'	73°16.12'	21		~91	+1/–4	SHRIMP	Very high U ≥ 2000 ppm, linear regression using U vs 206Pb/238 U Age gives ~90.5+1.1–3.6 Ma
FO98P10	Gabbro	Fiordo Nassau	47°56.35'	74°49.68'	13 of 16	0.61	85.7	1	SHRIMP	Some radiogenic Pb loss
FO0350a	Diorite	Punta Arauz	53°31.96'	72°21.16'	5 of 6	0.83	84.9	1	SHRIMP	For 5 of 6 analyses; 1 with radiogenic Pb loss
FO0331a	Granodiorite	Isla Desolacion E	53°20.70'	73°06.21'	5 of 6	0.98	84.7	1	SHRIMP	For 5 of 6 analyses — 1 older at ~100 Ma
FO98P28	Gabbro	Canal Montalva	47°48.67'	73°31.91'	11 of 11	0.55	84.0	1	SHRIMP	
FO0207	Granite	Punta Havana	53°09.40'	73°17.61'	27	–	–	–	SHRIMP	Significant scatter of the data, no clear-cut age grouping but more prominent are at 83 Ma and 78 Ma
FO0333a	Granodiorite	Punta Tilly	53°34.20'	72°24.19'	5 of 18	0.58	81.1	1	SHRIMP	For 5 of the 6 youngest analyses; considerable inheritance, up to ~500 Ma
FO98P27	Granite	Canal Gunter	47°50.94'	73°26.33'	8 of 10	0.54	78.7	1	SHRIMP	
FO0216	Diorite	Canal Silvia	52°58.45'	73°28.49'	9 of 19	0.35	77.9	1	SHRIMP	Significant scatter of data; appears to be three groupings and the more dominant is at 78 Ma — others are younger and ?radiogenic Pb loss
FO98P15	Granodiorite	Puerto Cueri Cueri	47°00.40'	74°12.48'	9 of 10	0.86	67.2	1	SHRIMP	
FO0329	Granodiorite	Punta Grup	52°54.33'	73°46.29'	13 of 13	2.00	64.3	1	SHRIMP	High MSWD; possibly a more dominant peak at 63 Ma with subordinate older group at 66 Ma
CA99-13	Granodiorite	Canal Adalberto	48°40.53'	74°34.36'			57.2	0.2	TIMS	Martin et al. (2001)
FO0039	Tonalite	Canal Guadalupe	51°12.10'	74°39.98'	5 of 12	0.04	56.5	1	SHRIMP	For 5 analyses forming a simple young peak
FO0205	Gabbro	Faro Felix	52°57.97'	74°04.41'	14 of 17	0.48	52.7	1	SHRIMP	For 14 analyses; one Ordovician area, some just slightly older
FO0040	Tonalite	Canal Smythe	51°45.180'	74°10.809'	7 of 10	0.43	49.9	1	SHRIMP	For 7 of 10 areas analysed; 3 older at ~53 Ma
FO0070	Gabbro	Canal Señoret	52°06.03'	74°14.11'	16 of 17	0.74	40.3	1	SHRIMP	For 16 of 17 analyses; one slightly older analysis
FO98P12	Monzodiorite	Fiordo Nassau	47°55.65'	74°47.11'	8 of 8	0.62	25.0	0.3	SHRIMP	
CA9914B	Gabbro–diorite	Canal Adalberto	48°36.26'	74°54.2'	10 of 11	0.43	23.1	0.3	SHRIMP	
FO0418	Granodiorite	Canal Artillería	50°24.91'	74°33.12'	10 of 11	1.08	22.6	0.3	SHRIMP	Dominant age group, minor older areas
FO0419	Volcanic breccia	Canal Artillería	50°30.74'	74°44.15'	6	–	–	–	SHRIMP	2 grains at ~22 Ma, others are Jurassic ~150 Ma
FO0202	Gabbro–diorite	I. Manuel Rodriguez	52°40.34'	73°45.61'	12 of 14	1.05	21.6	0.3	SHRIMP	For 12 of 14; one slightly older area and one younger
FO0211	Granodiorite	Puerto Gomez	52°58.51'	72°57.17'	18 of 20	1.40	20.6	0.2	SHRIMP	18 of 20 analyses, two just slightly older
IW9804	Granodiorite	Fiordo White	49°53.96'	74°36.58'	11 of 12	0.90	20.0	0.3	SHRIMP	
CE9924	Ultrabasic	Canal Erhart	48°44.95'	74°57.38'			20 and 120		SHRIMP	
FO0023	Tonalite	Bahia Inservible	50°46.90'	74°15.45'	14 of 15	0.75	19.8	0.2	SHRIMP	Minor radiogenic Pb loss
IW9803	Tonalite	Estero White	49°53.37'	74°37.10'	15 of 18	0.89	19.6	0.6	SHRIMP	One with radiogenic Pb loss leaving a slightly dispersed population, dominant age is 19.6 Ma
FO0010	Granite (altered)	Fiordo Asia	50°40.95'	73°47.10'	6 of 18	1.40	18.9	0.5	SHRIMP	Extreme U (many >>>3000 ppm), wtd mean for best <2000 ppm U
FO0013	Granodiorite	Puerto Tillman	50°30.50'	73°42.95'	15 of 18	2.10	18.8	0.2	SHRIMP	Some radiogenic Pb loss, some slightly older, dominant age grouping
FO0326	Tonalite	Canal Bambach	52°25.05'	73°45.59'	5 of 6	0.29	18.8	0.5	SHRIMP	For 5 of 6 analyses— 1 with radiogenic Pb loss
SE9804	Tonalite	Seno Europa	50°14.30'	73°00.60'	10 of 12	0.71	18.5	0.3	SHRIMP	
FO0042	Tonalite	Isla Piazzzi	51°45.456'	74°11.158'	9 of 9	0.17	18.4	0.9	SHRIMP	All 9 analyses, all high in common Pb; regression gives the same age
SE9803	Tonalite	Seno Europa	50°15.30'	73°59.21'	18 of 18	1.30	18.4	0.4	SHRIMP	Relatively simple population, may be some slightly older areas
FO0352	Granodiorite	Bahia Girior	53°24.61'	72°46.63'	6 of 6	0.89	18.0	0.6	SHRIMP	Simple magmatic age
FO98P2	Tonalite	Punta Daphne	47°36.37'	74°19.03'	16 of 17	1.13	16.4	0.3	SHRIMP	Minor radiogenic Pb loss
FO0019	Dacite	Isla del Medio	50°35.33'	73°45.10'	12 of 31	0.54	4.9	0.1	SHRIMP	Inheritance at 10 Ma, some radiogenic Pb loss and slightly older peak at 5.4 Ma
FO0408	Gneiss	Isla del Medio	50°28.26'	74°06.81'	8	–	–	–	SHRIMP	Scattered ages, ranging from ~160 Ma to ~985 Ma

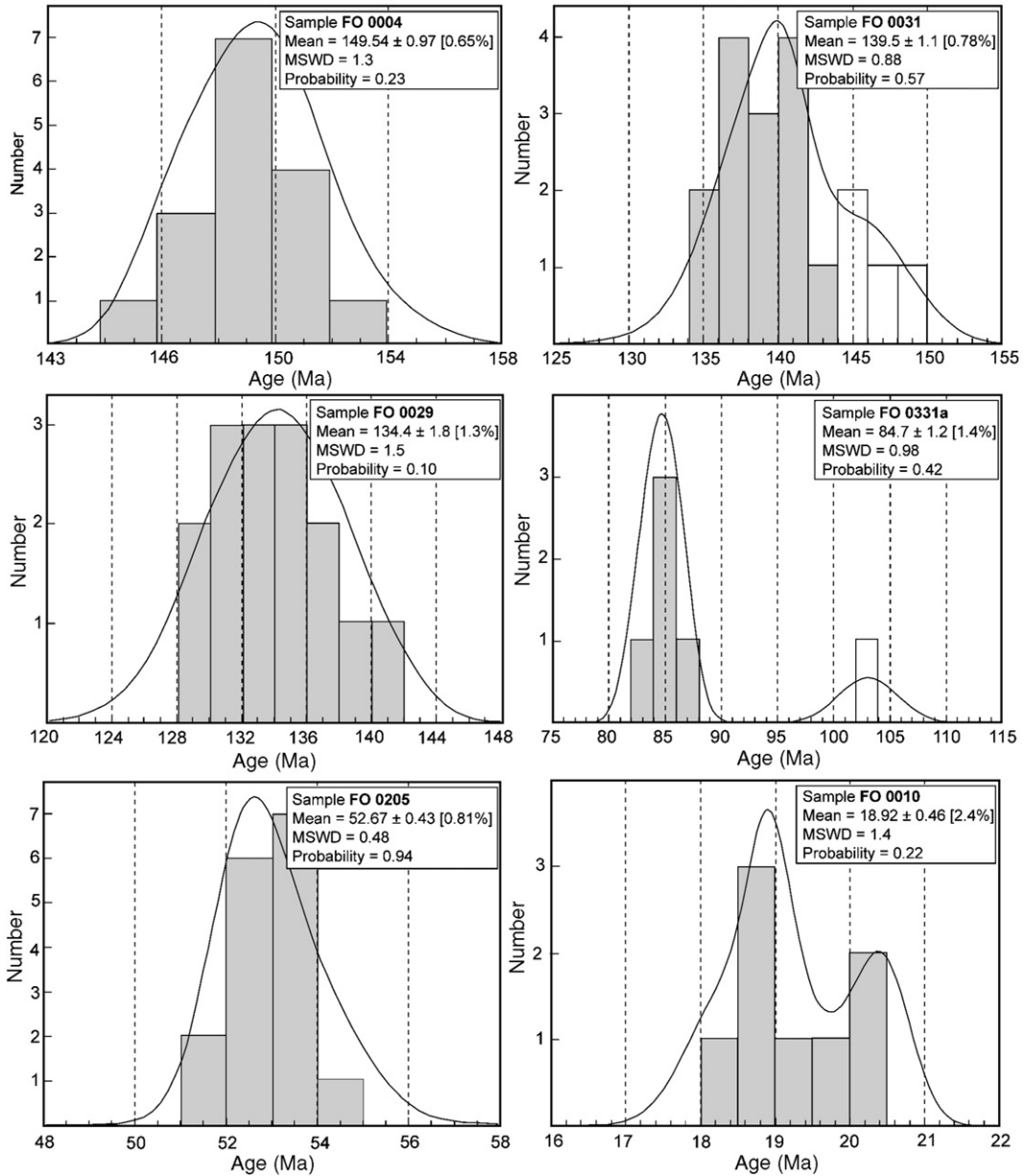


Fig. 3. Representative age vs relative probability diagrams for granitic rocks of the South Patagonian batholith. These include some samples with  $\sim 16$  analysed areas and others with 6 to 8 analysed areas, each area from different crystals. All ages quoted at 95% confidence level.

tuned to optimum sensitivity and to minimise production of interfering oxides species, with  $^{232}\text{Th}^{16}\text{O}/^{232}\text{Th}$  routinely  $\leq 0.5\%$ . The analyses were performed in peak hopping mode with a dwell time of 0.025 sec/mass. For each analysis the gas blank was acquired for 30 s, the laser triggered, and the signal acquired for a further 55 s. The analytical protocol essentially followed that of [Eggins et al. \(1998b\)](#). The primary calibrating standard was NIST-612 glass and the secondary standards were routinely analysed as unknowns as a check on data

quality control. Batches of analyses of 7 “unknowns” (SPB samples and secondary standards) were bracketed by analyses of NIST 612 allowing monitoring of, and correction for, instrumental drift. About 30% of samples were analysed 3 times as a check on glass homogeneity.

Data reduction used background corrected count rates and the method established by [Longerich et al. \(1996\)](#).  $^{29}\text{Si}$  was measured enabling use of XRF-determined  $\text{SiO}_2$  abundances as the internal reference element. Calibration values for NIST 612 used in the data

reduction are those of Eggin (2003). A linear drift correction based on the analysis sequence and on the bracketing analyses of NIST 612, was applied to the analyte count rate for each sample. Multiple analyses of the secondary standards indicated that analytical reproducibility and accuracy were better than 10% for nearly all reported elements, and better than 5% for most. An exception was Rb, which apparently partially evaporated from the sample during fusion. Rb data for standards and five samples analysed by XRF at BGS, Nottingham are on average 13% higher than obtained by ICP, so an empirical 13% increase was applied to the measured ICP analyses; Rb derived in this way is considered to be accurate to better than  $\pm 10\%$ . Sr contents were similarly compared to results obtained previously, and the raw ICPMS concentrations were reduced by 3% as a result.

### 5.3. Isotope analysis

Sr- and Nd-isotope determinations were carried out at NERC Isotope Geosciences Laboratory, UK, using the same chemical extraction techniques as were employed for the NPB (Pankhurst et al., 1999), with mass-spectrometric analysis on a multi-collector Finnegan MAT262. For Sm–Nd a  $^{150}\text{Nd}$ – $^{147}\text{Sm}$  mixed spike was used. The majority of Nd analyses employed mixed multi-channel peak jumping to eliminate gain effects, but recently simultaneous analysis was used; most of the Sr data were obtained by static multi-collection. Isotope compositions were normalised to  $^{146}\text{Nd}/^{144}\text{Nd}=0.7219$  and  $^{86}\text{Sr}/^{88}\text{Sr}=0.1194$ , and adjusted relative to an equivalent  $^{143}\text{Nd}/^{144}\text{Nd}$  value of 0.511867 for the La Jolla standard, and  $^{87}\text{Sr}/^{86}\text{Sr}=0.710230$  for NBS987.

## 6. Lithological constitution

The following descriptions are mainly based on the samples that have been dated by U–Pb zircon, but the extended collection of thin sections studied (ca. 250) shows no other rock types than those mentioned here, with the exception of scarce olivine-bearing gabbros. 72 modal analyses from the northern half of the SPB (Ureta, 2000), 62 from the Baker area (Weaver et al., 1990) and 46 from the Xaultegua area (Bruce et al., 1991) indicate overall proportions of 4% gabbro, 24% diorite, 52% tonalite and granodiorite and 20% granite in Streckeisen (1976) QAP plots (not shown). Study of the dykes is beyond the scope of this paper. More detailed lithological observations are presented below, after definition of the main chronological groupings.

## 7. Results

### 7.1. Geochronology

One of the surprising results of this study has been the importance and extent of Late Jurassic granitic magma emplacement within the batholith (Fig. 2). Ages in this group range from  $157\pm 3$  to  $144\pm 1$  Ma, mostly Kimmeridgian–Tithonian (Gradstein et al., 2004), so they are mostly coeval with the final stages of the V3 (157–153 Ma) rhyolites of the El Quemado and early Ibáñez formations (Pankhurst et al., 2000), although granite emplacement appears to reach a climax slightly later, at 150 Ma (Kimmeridgian–Tithonian boundary). The products of this initial magmatism are essentially confined to the eastern margin of the batholith including the anatectic monzogranite at Puerto Edén (Calderón et al., 2007). The Late Jurassic marginal belt is widest between the latitudes of Canal Andrés ( $\sim 50^{\circ}30'S$ ) and Península Muñoz Gamero ( $\sim 52^{\circ}20'S$ ); in the northern area it is only observed at the extreme head of Fiordo Baker (Bruce et al., 1991), and so far appears to be absent north of this and in the NPB. There is also a suggestion that the magmatism was initiated first in the south and spread towards the north, with the oldest age of  $157\pm 3$  Ma coming from just north of the Strait of Magellan.

Shortly after this the locus of plutonism jumped westwards. It is convenient to define a group of earliest Cretaceous granitoids, denominated Cretaceous 1, dated at 144–137 Ma (Berriasian–Valanginian), which occur mostly in the central parts of the archipelago, at least where the eastern Jurassic belt is well defined. In the northern area part of the SPB, these earliest Cretaceous granites are found near the eastern margin of the batholith. A second group of Early Cretaceous granitoids, Cretaceous 2, between 136 and 127 Ma, occurs mainly in the western margin of the batholith. A similar location of Early Cretaceous granitoids was observed in the North Patagonian batholith in the basis of Rb–Sr whole-rock isochrons (Pankhurst et al., 1999). In contrast, Late Cretaceous plutons (Cretaceous 3: 126 to 75 Ma) tend to occur in southern area of the batholith, between Bahía Xaultegua ( $52^{\circ}45'S$ ) and the southernmost point reached in the Strait of Magellan. Apart from this they were identified only sporadically at the western extremity of the Fiordo Baker section. Their overall low representation in the U–Pb database contrasts significantly with the acme of magmatism in this interval suggested by the earlier study of Bruce et al. (1991).

Post-Cretaceous granitoids in the SPB are subdivided into Palaeogene (67–40 Ma; 7 samples) and mostly

Neogene (25–15 Ma; 18 samples). They appear to indicate discrete events at the indicated intervals as in the North Patagonian batholith (Pankhurst et al., 1999) and are similarly confined to the axial region, between older units on either side.

At least six isolated Miocene alkaline to calc-alkaline plutons occur up to 70 km east of the margin of the SPB in an 800 km lineament sub-parallel to the present-day trench. The intrusion of these bodies was related by Michael (1991) to the subduction of the Chile Rise, which started at 14 Ma beneath the southern end of South America and since then has migrated northwards. It includes the Torres del Paine pluton (SHRIMP U–Pb zircon age  $12.65 \pm 0.13$  Ma, Sánchez et al., 2006). These bodies, which are undoubtedly related to subduction processes, are however not considered part of the SPB here, have not been studied in detail, and will not be treated further in this paper.

## 7.2. Lithological variation

### 7.2.1. Late Jurassic

The Late Jurassic plutonic rocks are predominantly leucogranites, the larger bodies of which are biotite-bearing non-porphyrific rocks, with roughly equal proportions of quartz, K-feldspar (perthitic orthoclase or microcline) and plagioclase, and with allanite, zircon and white mica as accessory phases. Associated amphibole gabbros contain abundant plagioclase and minor quartz, biotite, allanite, epidote and titanite. Igneous hornblende is commonly replaced by secondary amphibole, and plagioclase is sericitized. Although undated by us, garnetiferous two-mica monzogranites constitute the eastern portion of the SPB in Fiordo Baker (Ureta, 2000). Massonne et al. (2004) mention small intrusions and dykes containing magmatic garnet, muscovite and rare symplectites consisting of garnet–quartz or muscovite–plagioclase pairs formed by cotectic crystallization. Garnet compositions are typically close to the spessartine–almandine solid solution series and muscovites contain (10–17 mol.%) of celadonite component.

### 7.2.2. Cretaceous 1

The earliest Cretaceous plutons in the western margin of the batholith at Isla Duque de York and Isla Contreras, are mainly granodiorites and granites, but include some hornblende gabbros. The rocks tend to be porphyritic, with quartz and plagioclase phenocrysts, and biotite in smaller phenocrysts or in the medium- to fine-grained felsic groundmass, graphic in some samples. The accessory minerals are zircon, apatite, allanite and magnetite. Cumulate gabbros have plagioclase and poi-

kilitic hornblende phenocrysts in a plagioclase- and magnetite-rich groundmass.

### 7.2.3. Cretaceous 2

These are coarse-grained biotite–hornblende granodiorites and tonalites and minor pyroxene gabbros. Microcline is perthitic, quartz is usually polycrystalline. Accessory minerals are zircon, apatite, titanite and magnetite (up to 5%). Secondary minerals epidote, chlorite and prehnite are ubiquitous.

### 7.2.4. Cretaceous 3

The subsequent Cretaceous plutons at the southern end of the SPB are mostly coarse-grained biotite–hornblende tonalite and biotite granodiorite, with lesser amphibole gabbro and two-mica granite. They are foliated, contain epidote aggregates with biotite or amphibole, and recrystallized quartz. There are isolated occurrences in the Fiordo Baker area, in the extreme north of the area studied.

### 7.2.5. Paleogene

Paleogene plutons include the only two-clinopyroxene gabbros recognized in the SPB, together with magnetite-rich biotite–hornblende tonalites and granodiorites.

### 7.2.6. Neogene

The Neogene plutons are mainly medium- to coarse-grained hornblende–biotite tonalite and granodiorite. Two-mica garnet granite is present at Fiordo Peel, as well as a younger subvolcanic hornblende–plagioclase dacite porphyry (Fanning et al., 2001). A sub-ophitic hornblende gabbro is present at Canal Smith.

## 7.3. Geochemistry

Overall, as shown by our database of 103 whole-rock chemical analyses in R1R2 diagrams (Fig. 4), the batholith is composed of gabbro (12%), gabbro–diorite and diorite (26%), tonalite (15%), granodiorite (31%), and granite (16%). This is comparable to the distribution of rock types found by Bruce et al. (1991), our data set being poorer in gabbros and richer in granodiorite. Major and trace element chemical analyses of the dated samples are shown in Table 2 (supplementary data in Electronic annex EA-2).

### 7.3.1. Major and trace elements

Geochemical plots are presented for the dated rocks, selected from the broader data set and distinguishing between the six proposed age groups of rocks.

The entire suite shows a variation from gabbro to granite in the subalkaline field of the Cox et al. (1979) alkali–silica diagram (not shown). The Late Jurassic group shows a bimodal pattern, with predominant leucogranite and lesser amounts of gabbro and diorite. The earliest Cretaceous group shows a wide range of rock types with conspicuously lower alkali contents than the other groups. Intermediate granodiorite and tonalite tend to predominate in rocks from the Cretaceous 2, Cretaceous 3 and Neogene age groups, whereas the Paleogene rocks exhibit a higher proportion of gabbro and diorite. As is usual for calc–alkaline series rocks, the Harker variation diagrams (not shown) show good negative correlation between SiO<sub>2</sub> and Ca, Fe, Mg, Al and Mn, and more dispersed patterns in the alkalis, Ti and P<sub>2</sub>O<sub>5</sub>.

7.3.2. REE

Chondrite-normalized rare earth element (REE) data for the SPB are plotted in Fig. 5. The Late Jurassic granites show a well defined negative Eu anomaly not seen in the coeval gabbros. The Eu/Eu\* and [La/Yb]*n* ratios exhibit spatial variations within the age group, samples with different SiO<sub>2</sub> contents having similar patterns in a specific locality, but differing from those in other localities. The Cretaceous 1 rocks show well defined negative Eu anomalies only for rocks with more than 75% SiO<sub>2</sub>, and show a wide range in [La/Yb]*n* values and REE contents unrelated to SiO<sub>2</sub> content. The only two Cretaceous 2 and Cretaceous 3 rocks with

marked negative Eu anomalies have 68% and 74% SiO<sub>2</sub>, the latter with unusually low REE contents for the SPB suite. The rest of the rocks in the interval 52–72% SiO<sub>2</sub> have very subdued or even positive Eu anomalies. Paleogene rocks have positive or subdued Eu anomalies, except for one at 72% SiO<sub>2</sub>. None of the Neogene rocks has a marked negative Eu anomaly, but most have subdued ones throughout the chemical range.

7.3.3. Tectonic discrimination diagrams

In the Rb vs Y + Nb diagrams of Pearce et al. (1984), the SPB samples plot in the volcanic arc field, as expected (Fig. 6). However, the Late Jurassic samples tend to have higher Y and Rb contents, and thus plot nearer to the limit of the volcanic arc field than the rest of the rocks. Brown (1982) suggested that such enrichment in Rb, Th, U, Ta, Nb, Hf and Y and ‘impoverishment’ in Ba, Sr, P, Zr and Ti reflects the ‘maturity’ of a magmatic arc.

7.4. Isotope systems

Sr and Nd isotope and Sm–Nd data for 41 samples are reported in Table 3 and shown in Fig. 7. Due to the poor precision of the ICPMS analyses for Rb and Sr, initial <sup>87</sup>Sr/<sup>86</sup>Sr ratios (calculated from the U–Pb zircon ages as determined or implied by association with dated samples) are only reported where the age correction to the measured ratio is less than 0.001 (this mainly affects the Jurassic leucogranites, which have the highest Rb/Sr

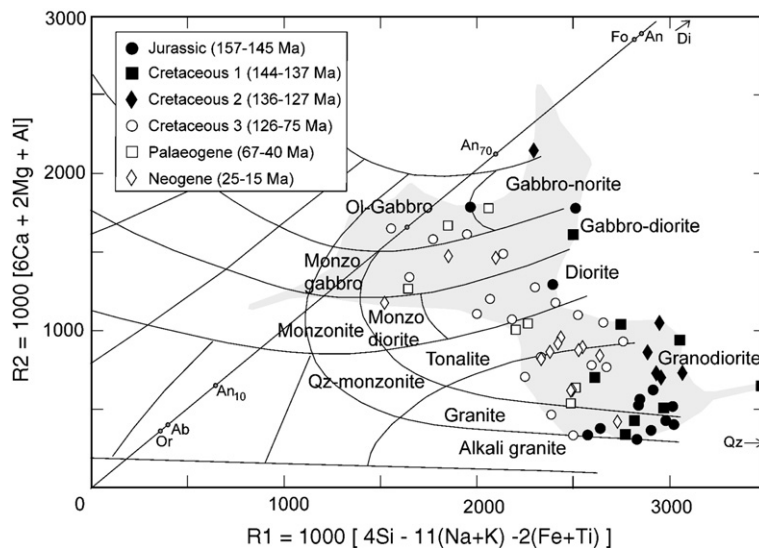


Fig. 4. Chemical classification of dated samples of the South Patagonian batholith in the R1R2 diagram of De la Roche et al. (1980). The shaded area represents the distribution of our extended geochemical database (Electronic annex EA-2). Symbols as in Fig. 2. Rock names used in this paper are derived from this plot.

Table 2  
Representative geochemical analyses of South Patagonian batholith granitoids

Locality	Fiordo Andrés			Canal Elías		Isla Contreras	Canal Elías
Sample No	F004-016	F00327A	F004-010	F00030	F00031	F00087	F00029
Lithology	D	GD	GD	GD	GbD	GbN	T
Age group	J	J	J	K1	K1	K2	K2
Age	148.8	148.3	151	139.9	139.5	135.9	134.4
SiO <sub>2</sub>	56.44	72.02	72.67	74.33	54.30	45.01	64.44
TiO <sub>2</sub>	1.03	0.20	0.20	0.18	0.42	0.60	0.62
Al <sub>2</sub> O <sub>3</sub>	15.12	14.08	13.58	13.24	16.99	23.46	15.24
Fe <sub>2</sub> O <sub>3</sub>	10.52	2.60	2.05	2.55	10.87	10.46	7.39
FeO							
MnO	0.18	0.05	0.03	0.02	0.20	0.15	0.11
MgO	3.75	0.47	0.36	0.37	4.76	3.53	1.68
CaO	7.36	2.39	2.16	3.34	9.69	13.79	6.16
Na <sub>2</sub> O	2.31	3.13	3.12	4.02	2.23	1.21	2.81
K <sub>2</sub> O	1.28	3.48	3.82	0.17	0.20	0.14	0.71
P <sub>2</sub> O <sub>5</sub>	0.18	0.05	0.05	0.05	0.10	0.03	0.16
SO <sub>3</sub>	0.02	0.02	0.02	0.02	0.03	0.52	0.09
F	0.03	0.04	0.05	0.03	0.02	0.02	0.04
Total	98.21	98.53	98.10	98.30	99.80	98.90	99.44
La	16.35	26.04	31.50	22.92	14.63	3.06	15.41
Pr	4.61	5.11	7.16	5.12	3.11	0.63	3.31
Ce	34.79	47.67	62.46	43.97	26.60	4.91	27.37
Nd	19.25	18.19	26.66	18.90	12.34	2.73	13.91
Sm	4.65	3.72	5.40	4.18	2.60	0.79	3.35
Eu	1.16	0.59	0.81	0.63	1.06	0.39	1.22
Gd	4.71	3.53	4.82	3.62	2.35	0.85	3.41
Dy	5.04	4.08	4.69	4.10	2.33	1.03	3.34
Ho	1.04	0.86	0.95	0.85	0.47	0.22	0.72
Tm	0.44	0.41	0.41	0.44	0.22	0.10	0.29
Er	3.08	2.73	2.85	2.76	1.42	0.65	2.03
Yb	3.03	2.98	2.72	3.03	1.51	0.68	1.90
Lu	0.46	0.45	0.42	0.48	0.24	0.10	0.29
Sc	36.82	10.83	8.91	8.31	40.86	38.26	24.17
Y	30.18	27.00	28.52	26.39	13.30	6.13	19.25
Zr	148.17	103.27	144.39	99.98	70.09	11.94	261.87
Nb	7.26	7.77	7.49	9.40	3.55	0.74	2.66
Ta	0.46	0.84	0.63	0.75	0.19	0.06	0.15
Ga	16.75	14.34	14.80	12.76	14.22	18.84	14.88
Rb	62.70	140.00	142.00	2.20	4.40	3.10	24.70
Sr	184.43	123.57	112.12	264.42	319.97	321.57	318.32
Ba	251.84	622.28	582.69	156.90	63.59	46.50	216.25
Th	3.39	13.63	13.45	10.55	1.84	0.87	2.22
Hf	3.49	2.95	4.16	2.98	1.64	0.37	5.04
U	0.87	2.18	1.97	1.74	0.34	0.22	0.50
Ti	6485.60	1178.16	1215.26	1100.66	2668.75	3657.40	4045.54

Major element oxides in wt.%; trace elements in ppm.

Lithology: G, granite; GD, granodiorite; T, tonalite; D, diorite; GbD, gabbro–diorite; GbN, gabbro–norite.

Age group: J, Jurassic (157–145 Ma); K1, Cretaceous 1 (144–137 Ma); K2, Cretaceous 2 (136–127 Ma); K3, Cretaceous 3 (126–68 Ma); Pal, Palaeogene (67–40 Ma); Neo, Neogene (<26 Ma).

ratios). Reliable initial  $^{87}\text{Sr}/^{86}\text{Sr}$  ratios are in the range 0.7032–0.7088, somewhat wider than the total range of 0.7036–0.7074 reported by Weaver et al. (1990) and significantly wider than that of 0.7037–0.7060 obtained

from Rb–Sr isochrons in the North Patagonian batholith by Pankhurst et al. (1999). Calculated  $\epsilon\text{Ndt}$  values range widely from +6.8 (for a 40 Ma old tonalite) to –7.0 (for one Jurassic granite).

<u>Punta Tilly</u>	<u>Punta Arauz</u>	<u>Bahía Barceló</u>	<u>Canal Bambach</u>	<u>Faro Felix</u>	<u>Fiordo Peel</u>	<u>Puerto Tilman</u>	<u>Bahía Inservible</u>
<u>F00333A</u>	<u>F00350A</u>	<u>F00351A</u>	<u>F00329</u>	<u>F00205</u>	<u>F00010</u>	<u>F00013</u>	<u>F00023</u>
<u>GD</u>	<u>D</u>	<u>G</u>	<u>GD</u>	<u>GbN</u>	<u>G</u>	<u>GD</u>	<u>T</u>
<u>K3</u>	<u>K3</u>	<u>K3</u>	<u>Pal</u>	<u>Pal</u>	<u>Neo</u>	<u>Neo</u>	<u>Neo</u>
81.1	84.9	94.1	64.3	52.7	18.9	18.8	19.8
66.97	62.95	50.70	71.36	51.03	74.28	66.50	61.65
0.31	0.29	1.07	0.36	0.69	0.11	0.43	0.62
16.06	19.15	17.57	14.01	21.08	13.91	15.06	14.94
4.18	3.46	10.66	2.47	7.24	1.35	3.70	5.96
0.07	0.10	0.21	0.07	0.12	0.10	0.08	0.12
0.65	1.04	4.32	0.71	4.29	0.25	1.86	2.11
3.89	5.92	9.28	2.05	10.51	1.22	4.04	4.83
3.92	4.02	2.98	4.26	3.10	3.57	3.47	3.32
1.77	2.16	1.20	3.08	0.30	4.04	2.23	1.86
0.08	0.15	0.31	0.09	0.09	0.05	0.13	0.11
0.02	0.03	0.02	0.02	0.02	0.02	0.02	0.02
0.06	0.05	0.04	0.03	0.01	0.04	0.02	0.03
97.97	99.32	98.35	98.50	98.47	98.91	97.54	95.55
21.58	12.57	16.16	28.06	4.01	16.02	25.99	26.29
4.76	2.91	4.11	5.26	1.07	3.37	4.20	6.26
40.40	23.90	31.47	49.36	7.47	29.81	41.77	51.57
17.54	11.70	17.75	17.82	5.08	12.67	14.04	24.71
4.12	2.56	4.11	3.34	1.41	2.80	2.32	5.21
0.93	0.86	1.24	0.71	0.87	0.47	0.68	1.19
4.19	2.24	3.86	2.77	1.56	2.71	1.83	4.50
5.16	2.17	3.37	2.84	1.63	3.10	1.58	4.21
1.10	0.44	0.67	0.59	0.34	0.60	0.33	0.84
0.53	0.20	0.27	0.30	0.15	0.28	0.14	0.36
3.42	1.36	1.90	1.86	1.03	1.86	0.97	2.48
3.80	1.44	1.81	2.19	1.07	1.94	1.02	2.46
0.58	0.23	0.27	0.36	0.16	0.29	0.15	0.36
14.28	7.06	24.80	6.95	25.30	3.94	8.80	17.04
34.48	13.52	19.42	18.83	9.95	20.55	10.01	25.41
161.16	114.46	73.67	240.41	21.72	54.63	77.83	171.84
9.70	4.79	5.73	13.38	0.96	9.39	9.31	10.95
0.92	0.32	0.31	1.12	0.06	1.22	0.80	0.71
17.63	16.60	18.56	13.87	16.46	13.93	14.91	16.33
78.20	61.80	44.40		5.90		110.20	72.70
209.97	796.93	557.59	180.07	475.59	123.65	367.07	410.87
475.10	635.70	327.55	546.23	100.76	576.26	398.47	552.10
10.72	4.47	4.25	11.25	0.48	10.12	15.41	9.93
4.57	2.82	1.94	5.28	0.64	1.74	2.24	4.41
2.98	1.15	1.05	2.35	0.14	1.82	2.24	1.63
1928.33	1778.49	6787.78	2206.52	4251.75	531.13	2638.39	4725.37

There is a clear age progression in isotope compositions (Fig. 8). Jurassic granitoids have rather high initial  $^{87}\text{Sr}/^{86}\text{Sr}$  ratios of 0.7068–0.7092 (mean 0.7080, based on five values considered reliable) and negative  $\epsilon\text{Ndt}$

values of  $-4.2$  to  $-7.0$  (mean  $-5.2$ ). The earliest Cretaceous group is only slightly more juvenile in Sr and Nd isotope compositions, with values of 0.7068–0.7088 (mean of six = 0.7074) and  $-2.5$  to  $-4.4$  (mean  $-3.6$ ).

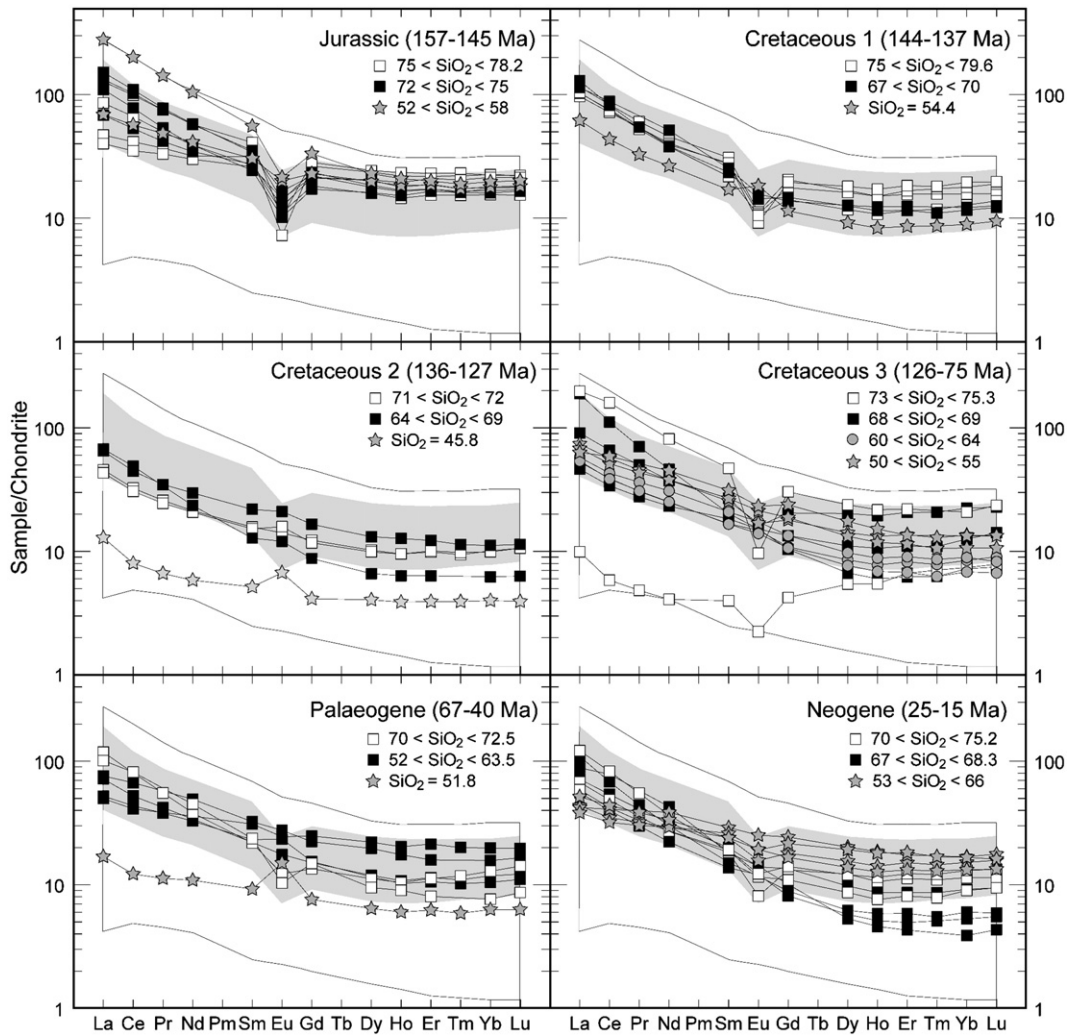


Fig. 5. Chondrite normalized REE diagrams (Sun and McDonough, 1989) for the dated rocks of the South Patagonian batholith by the age categories defined in the text. In all diagrams the light continuous line indicates the extreme values of all the geochemical data set, and the light shaded areas the limit for 80% of the samples.  $\text{SiO}_2$  values on anhydrous basis.

The three Cretaceous 2 granitoids analysed are clearly distinguished from these early products, with initial  $^{87}\text{Sr}/^{86}\text{Sr}$  ratios of 0.7048–0.7053 (mean 0.7051) and mostly near zero  $\epsilon\text{Ndt}$  values of  $-1.3$  to  $-0.1$  (mean  $-0.7$ ). Late Cretaceous 3 granitoids have initial  $^{87}\text{Sr}/^{86}\text{Sr}$  ratios of 0.7039–0.7047 (mean of nine = 0.7042) and mostly positive  $\epsilon\text{Ndt}$  values of  $-0.5$  to  $+4.0$  (mean  $+1.9$ ). The most primitive values of all are shown by the Palaeogene granitoids (0.7036–0.7040 and  $+4.1$  to  $+6.8$ , respectively), whereas in the Neogene isotope compositions resemble those of the Late Cretaceous rocks (0.7037–0.7048 and  $-0.5$  to  $+5.1$ ).

The distribution in the  $\epsilon\text{Sr}$ – $\epsilon\text{Nd}$  plot follows conventional S–I type trends from long-term LIL-enriched to LIL-depleted sources (Fig. 7). Compared to an equiv-

alent database for the North Patagonian batholith (Pankhurst et al., 1999), there is a marked extension into the LIL-enriched (crustal sources) quadrant. When plotted against crystallization age (Fig. 8) it is apparent that this is due entirely to the extension of the age spectrum in the SPB to ages over 150 Ma, since these Late Jurassic granitoids are absent from the North Patagonian batholith. Data for the two batholiths match remarkably closely for ages younger than 140 Ma.

## 8. Discussion

Overall, the chemical composition of the rocks in our database differs somewhat from the assessment of Bruce et al. (1991) in terms of percentage of basic (15%),

intermediate (33%) and acid (52%) rocks. However, their study was based on more restricted sample areas, and biased towards the Mid to Late Cretaceous rocks in the Xaultegua region. The inclusion in our data set of the Late Jurassic granitoids, which were not considered by Bruce et al. (1991), suggests that the above percentages are a better representation of the lithological constitution of the SPB as a whole. Our geochronology data set, based on 56 rocks dated by U–Pb on zircon, is somewhat biased towards the acid compositions by the Late Jurassic component. However, the age distribution of Bruce et al. (1991), based mainly on K–Ar and Ar–Ar ages, which showed a peak of igneous activity between 70 and 120 Ma cannot be sustained in the light of our data. The differences can be explained by the geographically restricted sampling and the K–Ar dating methods used, which are prone to give cooling ages instead of igneous crystallization ages. Calderón (2005), for example, has shown that in the Puerto Edén area, rocks with ca. 150 Ma zircon ages yield ca. 100 Ma K–Ar ages in biotite. We suggest that the Mid to Late Cretaceous peak of Bruce et al. (1991) may be greatly influenced by the tectonic evolution of the area, in which a well documented mid-Cretaceous compressive tectonic event (Dalziel, 1981; Fildani et al., 2003) may have caused exhumation and partial cooling of the SPB. Our estimates of both age and composition variations may be more biased towards the Jurassic granitoids of the eastern margin (albeit unintentionally), but nevertheless we consider that they are more representative of the SPB as a whole.

### 8.1. Interpretation of changes in geochemistry and isotope composition with time

As shown emphatically by U–Pb SHRIMP chronology, the Late Jurassic granites in the main body of the SPB are volumetrically very important; they constitute ca. 25% of the SPB, concentrated at the eastern margin of the batholith. They are also exceptional in the sense that there are voluminous silicic volcanic rocks of similar age and geochemistry, the Tobífera Formation, which crop out extensively east of the SPB. There is no systematic dating or isotopic study of the Tobífera, but recent SHRIMP data (Calderón et al., 2004; Calderón, 2006) suggest that it was erupted in Late Jurassic times (casting doubt on the age of  $171.8 \pm 1.2$  Ma reported by Pankhurst et al., 2000) contemporaneously with, but also continuing to later than, other V3 rhyolitic formations dated at 157–153 Ma (El Quemado and Ibáñez formations). Sr isotope systematics in these Andean rhyolites are significantly disturbed by later hydrothermal or deformational events, but eight unpublished analyses of the El Quemado Formation have apparent initial  $^{87}\text{Sr}/^{86}\text{Sr}$  ratios at 156 Ma of 0.7047–0.7112 (mean  $0.7075 \pm 0.0022$ ) and  $\epsilon_{\text{Ndt}}$  values of  $-2.0$  to  $-5.6$  (mean  $-4.3 \pm 1.2$ ). The Jurassic rhyolites of Patagonia and the Antarctic Peninsula have been interpreted as dominated by lower crustal melts derived from low-Rb/Sr ratio material of possibly late Mesoproterozoic age, albeit with an increasing subduction-related component in time and proximity to the proto-Pacific margin (Gust et al., 1985; Pankhurst and Rapela,

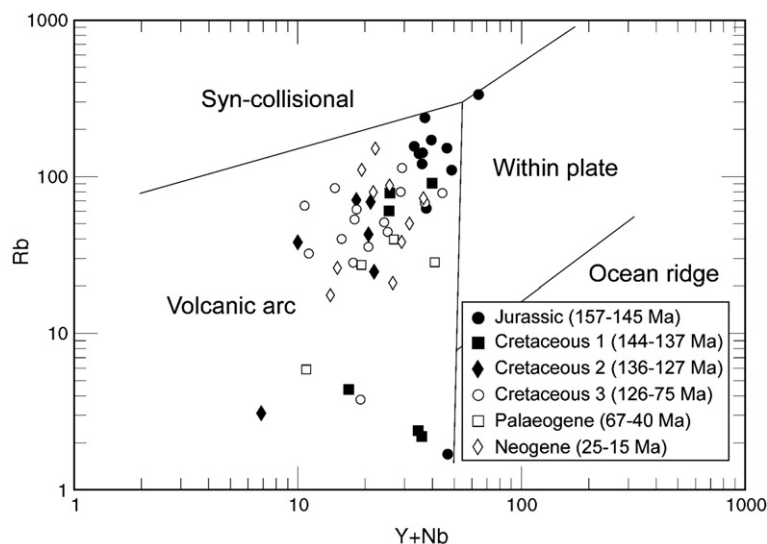


Fig. 6. Tectonic discrimination diagram of Pearce et al. (1984) for the SHRIMP U–Pb zircon dated rocks of the South Patagonian batholith. Symbols as in Fig. 2.

Table 3  
New Nd and Sr isotope data for the South Patagonian batholith

Sample	Lithology	Age Ma	Sm ppm	Nd ppm	$^{147}\text{Sm}/^{144}\text{Nd}$	$^{143}\text{Nd}/^{144}\text{Nd}$	(Nd $^{143}$ / Nd $^{144}$ ) <sub>t</sub>	$\epsilon\text{Nd}_t$	TDM* Ma	Rb ppm	Sr ppm	$^{87}\text{Rb}/^{86}\text{Sr}$	$^{87}\text{Sr}/^{86}\text{Sr}$	( $^{87}\text{Sr}/^{86}\text{Sr}$ ) <sub>t</sub>	$\epsilon\text{Sr}_t$
<i>Late Jurassic</i>															
FO0105	Granite	152	4.947	15.220	0.1965	0.512351	0.512156	-5.6	1414	334.3	37.3	26.025	0.747757		
FO0015	Associated rhyolite	152*	5.302	19.848	0.1615	0.512316	0.512155	-5.6	1414	110.1	202.1	1.577	0.712619	0.709212	69.47
FF9909A	Granodiorite	151*	5.732	25.641	0.1351	0.512307	0.512173	-5.3	1389	171.3	136.6	3.631	0.716589		
SI9929	Diorite	150*	5.666	26.203	0.1307	0.512317	0.512189	-5.0	1368	11.6	231.3	1.447	0.709917	0.706832	35.65
SI9930A	Granodiorite	150*	4.080	19.112	0.1291	0.512329	0.512202	-4.7	1348	126.5	161.9	2.262	0.712327	0.707505	45.20
SI99230B	Enclave	150*	3.906	12.381	0.1907	0.512374	0.512187	-5.0	1371	147.3	150.3	2.837	0.713702	0.707653	47.30
FO0009	Foliated leucogranite	150	6.557	30.209	0.1312	0.512292	0.512163	-5.5	1405		64.7		0.720035		
SE9811	Leucogranite	150	6.160	35.803	0.1040	0.512276	0.512174	-5.3	1390	129.0	142.1	2.628	0.714368	0.708765	63.10
FO0054	Leucogranite	149	4.266	22.754	0.1133	0.512344	0.512234	-4.2	1303	156.2	99.8	4.531	0.716996		
FO0004	Granite	149	5.046	17.829	0.1711	0.512395	0.512228	-4.3	1311	152.1	73.4	6.003	0.718510		
PE9932A	Gneissic granite	149	5.138	25.967	0.1196	0.512203	0.512086	-7.0	1515						
<i>Earliest Cretaceous</i>															
FO0037	Leucogranite	143	4.357	20.596	0.1279	0.512374	0.512254	-3.9	1280	90.5	138.7	1.889	0.710643	0.706804	35.13
FO0038	Leucogranite	141	2.509	13.463	0.1126	0.512339	0.512235	-4.3	1311	78.4	151.4	1.498	0.710389	0.707386	43.36
FF9910C	Porphyritic granodiorite	140	6.811	32.526	0.1266	0.512381	0.512265	-3.8	1268	159.4	107.1	4.311	0.717207		
FF9910A	Epidote granite	140*	5.865	29.455	0.1204	0.512389	0.512279	-3.5	1247	2.4	342.5	0.021	0.708820	0.708779	63.12
FO0030	Porphyritic granite	140	4.085	20.094	0.1229	0.512441	0.512328	-2.5	1171	2.2	256.4	0.024	0.707079	0.707030	38.29
FO0031	Diorite	140	2.475	12.106	0.1236	0.512424	0.512311	-2.9	1198	4.4	310.3	0.041	0.707356	0.707274	41.76
FO0029	Tonalite	135	3.318	14.687	0.1366	0.512518	0.512397	-1.3	1069	24.7	308.7	0.231	0.705559	0.705115	11.02
CA9916A	Foliated granodiorite	138	3.579	19.077	0.1134	0.512335	0.512335	-4.4	1318	60.4	206.7	0.846	0.708925	0.707265	41.60
EC9918	Leucogranite	136	2.035	11.020	0.1116	0.512532	0.512433	-0.6	1011	38.0	315.7	0.348	0.705430	0.704758	5.96
<i>Mid to Late Cretaceous</i>															
FO0089	Granodiorite	130	2.046	8.401	0.1472	0.512589	0.512464	-0.1	968	42.7	302.8	0.408	0.706047	0.705293	13.46
FO0218a	Tonalite	126	1.394	4.648	0.1814	0.512830	0.512680	4.0	592	53.4	410.7	0.376	0.704543	0.703869	-6.83
SI9925	Granodiorite	122	2.776	10.592	0.1585	0.512618	0.512492	0.2	934	113.8	510.4	0.645	0.705372	0.704254	-1.43
FO0072b	Tonalite	114	1.118	5.360	0.1262	0.512558	0.512464	-0.5	991	65.4	355.4	0.532	0.705565	0.704703	4.81
FO0222b	Tonalite	100	2.865	15.496	0.1118	0.512679	0.512606	1.9	771	35.6	653.2	0.158	0.704290	0.704066	-4.47
FO0065	Tonalite	95	4.031	18.253	0.1335	0.512707	0.512624	2.1	746	79.7	440.9	0.523	0.705044	0.704338	-0.69
FO98P10	Diorite	86	2.872	12.585	0.1380	0.512659	0.512581	1.1	835	3.8	889.5	0.012	0.704657	0.704642	3.47
FO0331a	Granodiorite	85	1.397	6.916	0.1221	0.512745	0.512677	2.9	667	32.2	891.3	0.104	0.704257	0.704131	-3.80
FO0207	Leucogranite	83	0.539	2.391	0.1363	0.512714	0.512640	2.1	737	84.4	458.3	0.532	0.704829	0.704201	-2.84
FO0216	Granodiorite	78	4.559	23.291	0.1183	0.512782	0.512722	3.6	596	67.8	476.1	0.412	0.704446	0.703989	-5.93
<i>Paleogene</i>															
CA9913	Granodiorite	57.2	3.511	14.767	0.1437	0.512854	0.512800	4.6	482	20.2	457.2	0.128	0.703679	0.703575	-12.16
FO0039	Diorite	56.5	4.304	16.275	0.1599	0.512833	0.512774	4.1	534	28.4	336.9	0.244	0.704209	0.704013	-5.96
FO0205	Diorite	52.8	1.042	3.900	0.1615	0.512847	0.512791	4.3	508	5.9	461.2	0.037	0.703876	0.703848	-8.36
FO0070	Tonalite	40.3	3.500	15.581	0.1358	0.512973	0.512937	6.8	234	27.3	452.7				
<i>Neogene</i>															
FO0202	Granodiorite	21.2	3.493	15.645	0.1350	0.512889	0.512870	5.1	409	20.9	518.1	0.117	0.703750	0.703715	-10.79
FO0211	Granodiorite	20.6	3.307	22.171	0.0902	0.512628	0.512616	0.1	874	150.7	236.6	1.842	0.705220	0.704681	2.92
FO0023	Granodiorite	19.8	4.482	19.021	0.1425	0.512802	0.512784	3.3	579	72.7	398.4	0.528	0.704242	0.704093	-5.44
FO0010	Altered granite	18.9	1.591	6.506	0.1478	0.512606	0.512588	-0.5	923		119.9		0.706127		
FO0326	Granite	18.8	2.483	12.098	0.1241	0.512823	0.512808	3.8	535	47.9			0.704044		
FO0013	Granodiorite	18.8	2.432	14.628	0.1005	0.512752	0.512740	2.5	661	110.2	356.0	0.895	0.704356	0.704117	-5.12
FO98P2	Granodiorite	16.4	2.412	14.090	0.1035	0.512788	0.512777	3.1	597	17.6	813.5	0.062	0.703962	0.703947	-7.57

TDM\* = variable crust Sm/Nd multistage model age after DePaolo et al. (1997).

( $^{87}\text{Sr}/^{86}\text{Sr}$ )<sub>t</sub> calculated only where age correction is reasonable. Italics: Rb and Sr values corrected as indicated in the Geochemistry section of text.

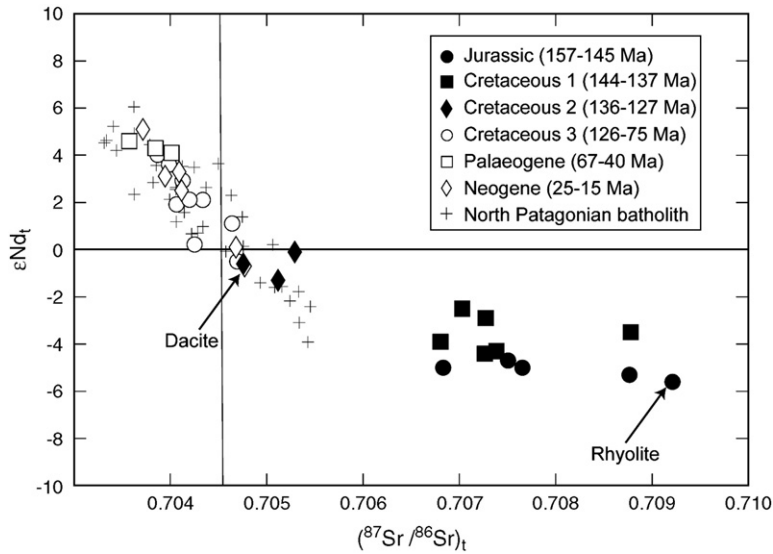


Fig. 7. Comparison of  $\epsilon Nd_t$  vs  $(^{87}Sr/^{86}Sr)_t$  values from the South Patagonian batholith and from the North Patagonian batholith (NPB) (Pankhurst et al., 1999). The Jurassic and Cretaceous 1 values from the SPB have no counterpart in the NPB, both batholiths having otherwise similar trends and values in the diagram for younger rocks.

1995; Pankhurst et al., 2000; Riley et al., 2001). The rhyolites formed by explosive eruptions which covered large areas and were in part deposited in the initial stages of the developing Rocas Verdes basin, where they are now preserved. The geochemical and isotopic characteristics of the Late Jurassic SPB leucogranites strongly suggest a common petrogenesis with these rhyolites, and the presence of gabbros in the association is consistent with subduction-generated magmatism. However,

the petrochemical data obtained do not clearly establish whether the Late Jurassic SPB leucogranites were formed in a subduction-related arc to the west of the Rocas Verdes basin, or if they are the result of the extension-related bi-modal magmatic activity. Our data also suggest that the earliest Cretaceous SPB granitoids, emplaced outboard of the Jurassic belt, represent the final stage of this vastly extensive and long-lived magmatic episode.

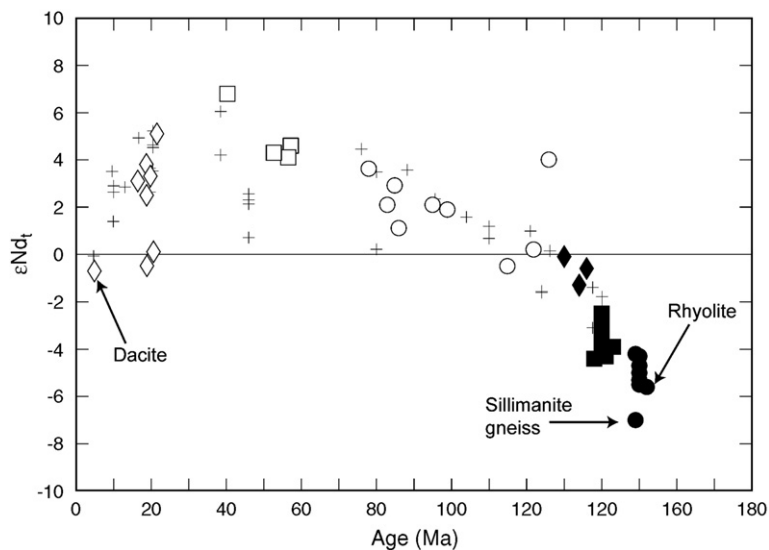


Fig. 8.  $\epsilon Nd_t$  vs age plot of dated samples from the South Patagonian batholith and from the North Patagonian batholith (NPB) (Pankhurst et al., 1999). Symbols as in Fig. 7. Within similar overall trends, differences between the SPB and NPB seem greater in the Cenozoic rocks.

Subsequent SPB magmatism is of a markedly different nature, dominated by granodiorites and diorites from LIL-depleted mantle sources. The distribution of these granitoids is generally more restricted — Cretaceous in the southern sector, Paleogene and Neogene along the axis of the batholith. Volcanic rocks of ages similar to the Cretaceous and Cenozoic components of the SPB are entirely lacking within the margins of the batholith, with the exception of little-known volcanic breccias of Miocene age (sample FO0419, Table 1). In the Magallanes basin to the east of the batholith, the only Cretaceous volcanic rocks are mainly submarine basaltic breccias of the Barros Arana Formation (Prieto, 1987), which have a K–Ar age of 104 Ma (Stern et al., 1991). These have an alkaline geochemical affinity and were erupted independently of the SPB activity. Cretaceous and Paleogene volcanic rocks were probably very much reduced in volume compared to the Jurassic, and confined to the area of the exposed SPB, from where they have been completely eroded. During the Miocene, explosive volcanism took place again, and its deposits are found in the Magallanes Basin, including air fall tuffs as far as 200 km east of the present margin of the SPB (Hervé et al., 2004; Casanova, 2005).

We speculate that the Late Jurassic granites, and probably also the Neogene granites, might represent development of large magma bodies in the lower to middle crust, giving rise to conditions appropriate to the generation of large caldera-forming eruptions. It is possible to conceive that this large magma accumulation at mid-crustal levels, and its associated large ignimbrite eruptions, represent a situation similar to the one described in the present-day Central Andes (Wigger et al., 1994; Yuan et al., 2000), in which the Andean Low Velocity Zone, supposedly representing an unusually high proportion of magma, gives rise to the voluminous late Cenozoic silicic ignimbrites of the Altiplano region. On the other hand, from the Cretaceous 2 to the Paleogene the plutons might have formed incrementally (Glazner et al., 2004), largely through dyke-like emplacement and without the appropriate conditions for large caldera eruptions. The former situation requires that the thermal input of magmas exceeds the rate of thermal loss by cooling and eruption, whereas the latter requires that the thermal input is low, with cooling preventing the development of a large magma body within the crust, so that plutons may form by successive injection of smaller magma batches. Field observations in support of the latter situation can be observed in Canal Elías, where vertical decametric bodies of different plutonic lithologies and almost identical U–Pb SHRIMP zircon ages have cross-cutting relationships. The negative or near to zero  $\varepsilon_{\text{Nd}}$  values of the Late

Jurassic and Cretaceous 1 granitoids (as well as some of the Neogene granites), in contrast with positive ones for the Cretaceous 3 and Paleogene could reflect the larger degree of crustal contamination of the magmas expected in large long-lived magma chambers than in smaller and faster cooling plutons.

It is apparent in Fig. 7 that the Late Jurassic plutons in the SPB have no equivalent in the NPB, at least in its main body. The SPB spans the latitudes where the Madre de Dios exotic terrane collided with the western margin of Gondwana (Forsythe and Mporozis, 1983; Rapalini et al., 2001). The collision must have taken place between Middle Permian and earliest Jurassic (Thomson and Hervé, 2002), probably closer to the younger limiting age, when metamorphic rocks cooled through zircon and apatite FT closing temperatures, indicating rapid uplift and denudation. This might have produced a locally somewhat thickened crust in the collision zone, thus enhancing the possibility of increased crustal melting in this area during initiation of the subduction process, within the otherwise extensional tectonic setting of southern Patagonia in the Late Jurassic. The Cretaceous 2 western margin to the SPB records its emplacement in the Madre de Dios terrane, but the Late Jurassic eastern margin at Seno Andrés intrudes marble bodies (undetected until this study) that are equally characteristic of the Madre de Dios terrane.

The Rocas Verdes basin, with its quasi-oceanic floor represented in the studied area by the Sarmiento ophiolitic complex, has been interpreted as a back-arc basin (Dalziel and Cortés, 1972; Dalziel et al., 1974; Stern and de Wit, 2003) generated by extension behind the magmatic arc whose roots are represented by the SPB. Sparse radiometric dating of Rocas Verdes rocks from South Georgia to Sarmiento has suggested that the mafic floor was revealed by ‘unzipping’ of the continental crust from south to north. As noted above, there is also a suggestion that SPB magmatism was initiated first in the south and spread towards the north. Our field observations show that Late Jurassic acid dykes intruded the western margin of the ophiolite complex, and undated mafic dykes considered to represent Rocas Verdes magmatism intrude Late Jurassic granitic rocks within and west of the complex. This implies that the Late Jurassic components of the SPB were emplaced both before and after the mafic magmatism of the Sarmiento ophiolitic complex. This is also consistent with the termination of ophiolitic magmatism before the late Tithonian deposition of the Zapata Formation (Fuenzalida and Covacevich, 1988). The western margin of the ophiolite complex, mainly consisting of pillow basalts, forms a thrust sheet with eastern transport (Calderón, 2006), indicating that

the original east–west extent of the basin exceeded its present-day outcrops, by an unknown amount. The complex is considered to be a supra-subduction zone ophiolite, generated in an extensional tectonic regime, which should thus also have been the tectonic setting for the emplacement of the Late Jurassic components of the SPB. It is probable that the Rocas Verdes basin was generated at or near the suture zone between the Madre de Dios terrane and Gondwana.

There remains confusion over the origins of granitoid magmas, mostly related to their isotopic compositions. There are two restrictions that need to be stated clearly. The first is that batholithic magmas of predominantly intermediate composition cannot be formed directly by fusion of mantle material, and the predominance of intermediate over gabbroic rocks in the batholiths cannot result simply from fractional crystallisation. Even if ultimately derived from the mantle, with little isotopic input from the crust, successive crystallisation and partial re-melting is required and this has to be a process that takes place within, or near the base of, the crust. Second, the occurrence of large volumes of magma with relatively homogeneous crustal isotopic signatures can result either from the anatexis of uniform mature crust of the appropriate composition, or a restricted range of mixing between mantle and crustal components. The latter has generally been more favoured in published models, although the contamination process would have to be closely buffered to result in the uniformity of isotopic compositions observed here along vast lengths of the batholith margin. Judging by the evidence that some Late Jurassic leucogranites of the SPB crystallised at depths of 20 km (Massonne et al., 2004), magma formation must have occurred at a deeper level, in the lower crust.

## 9. Conclusions

The South Patagonian batholith, a major part of one of the largest Cordilleran batholiths on Earth, was formed over a period of 150 m.y. Its construction, as a result of subduction of Pacific Ocean floor beneath the South American plate, was not continuous, but episodic. One of the most intense episodes occurred at the initial stage in Late Jurassic times, when bimodal leucogranite–gabbro bodies were emplaced along the western Gondwana margin. The magmas that generated these granitoids were contemporaneous, and probably cogenetic, with the final stages of the extensive rhyolite volcanism associated with the continental rifting and break-up. The principle mechanism envisaged for Jurassic magmatism in Patagonia is anatexis of the continental lithosphere, possibly involving

an old mafic lower crust. In earliest Cretaceous times the same magma generation process continued, albeit with magmas diluted slightly by incorporation of melts from more depleted mantle and/or reduction of the crustal component, but the locus of emplacement shifted westwards, to a position outboard of the Late Jurassic belt. From 137 Ma onwards, the subduction-related magmas were generated in increasingly more depleted mantle (indicated by the continual occurrence from this time onwards of mafic dykes within the batholith). This change appears to coincide with initial opening of the South Atlantic Ocean and the start of closure of the Rocas Verdes basin, possibly reflecting the effect of accelerated westward drift of the continent on Pacific subduction. Cretaceous 2 and Cretaceous 3 granitoids (typically tonalite and granodiorite) were locally voluminous, but account for rather less of the exposed batholith than has been previously thought. Cretaceous 2 plutons form the western margin of the SPB and the late Cretaceous 3 plutons are apparently largely restricted to the southern sector of the SPB, between the two earlier belts. The most primitive magmas, geochemically and isotopically, were those responsible for the restricted occurrence of Paleogene granitoids, which include two-pyroxene gabbros. These were emplaced along the axis of the batholith, as were the far more voluminous Neogene tonalite–granodiorites, with occasional dacites. This last recognisable stage is characterised by a return to slightly more evolved isotopic signatures, which indicates renewed involvement of crustal sources, although by this stage such sources would also have included the previously crystallised batholithic rocks. As in the Late Jurassic, the Neogene granitoids were contemporaneous with widespread volcanism.

Formation of the batholith was not a continuous process, and we see no evidence for a gradual change from isotopically evolved to isotopically primitive compositions that should result from either the increasing sealing of magma–crust interface (Weaver et al., 1990; Bruce et al., 1991) or the selective removal of an easily fusible melt fraction from an initially fertile mantle source (Leat et al., 1995). We propose that the changes of magma composition in time resulted from episodic changes in tectonic conditions that mostly affected the rate of magma generation, and this was the crucial factor, related to the ability to form large magma chambers in which isotopic homogenisation of mantle and crustal components could occur.

## Acknowledgements

Field and laboratory studies have been funded by FONDECYT projects 1010412, 7010412, 1050431 and

7060240. Captains Conrado Alvarez, Sr and Jr., have taken us safely in the yachts Penguin and Foam to these remote areas. Field collaboration and discussion from S. Thomson, H. Bahlburg, C. Augustsson, J. Bradshaw, U. Cordani, A. Fildani, J. Munhá, P. Fonceca, M. Suárez, R.A.J. Trouw and the Universidad de Chile geology students M. Solari, E. Dzogolyk, V. Faúndez, C. Herrera, G. Galaz and C. Ramírez are greatly appreciated. Thorough reviews by Allen Glazner and an anonymous referee contributed significantly to the improvement of the final manuscript.

## Appendix A. Supplementary data

Supplementary data associated with this article can be found, in the online version, at [doi:10.1016/j.lithos.2007.01.007](https://doi.org/10.1016/j.lithos.2007.01.007).

## References

- Brown, G.C., 1982. Calc-alkaline intrusive rocks: their diversity, evolution and relation to volcanic arcs. In: Thorpe, R.S. (Ed.), *Andesite, Orogenic Andesite and Related Rocks*. John Wiley and Sons, Chichester, pp. 437–461.
- Bruhn, R.L., Dalziel, I.W.D., 1977. Destruction of the Early Cretaceous marginal basin in the Andes of Tierra del Fuego. In: Talwani, M., Pitman, W.C. (Eds.), *Island Arcs, Deep Sea Trenches, and Backarc Basins*. AGU Maurice Ewing Series, vol. 1, pp. 395–405.
- Bruhn, R.L., Stern, C.R., de Wit, M.J., 1978. Field and geochemical data bearing on the development of a Mesozoic volcano-tectonic rift zone and back-arc basin in southernmost South America. *Earth and Planetary Science Letters* 41, 32–46.
- Bruce, R.M., Nelson, E.P., Weaver, S.G., Lux, D.R., 1991. Temporal and spatial variation in the southern Patagonian batholith: constraints on magmatic arc development. In: Harmon, R.S., Rapela, C.W. (Eds.), *Andean Magmatism and its Tectonic Setting*. Special Paper, Geological Society of America, vol. 265, pp. 1–12.
- Calderón, M., 2000. *Metamorfismo de contacto en el margen oriental del Batolito Patagónico, entre los 48° y 50°30' Lat. S., Magallanes, Chile*. Graduation Thesis, Departamento de Geología, Universidad de Chile.
- Calderón, M., 2005. *Metamorfismo de alta temperatura y baja presión en rocas del basamento metamórfico en Puerto Edén*. MSc Thesis, Departamento de Geología, Universidad de Chile, 103 pp.
- Calderón, M., 2006. *Petrogenesis and tectonic evolution of Late Jurassic bimodal magmatic suites (Sarmiento Complex) and migmatites (Puerto Edén Igneous Metamorphic Complex) in the southern Patagonian Andes, Chile*. PhD Thesis, Departamento de Geología, Universidad de Chile, 170 pp.
- Calderón, M., Hervé, F., 2000. *Metamorfismo de contacto en el margen oriental del batolito sur patagónico (48°–50°30'S)*. IX Congreso Geológico Chileno 2, 707–711.
- Calderón, M., Hervé, F., Fanning, C.M., 2004. Late Jurassic birth of the Rocas Verdes Basin at the Sarmiento Ophiolitic Complex: evidence from Zircon U–Pb SHRIMP geochronology. In: Carcione, F., Donda, F., Lodolo, E. (Eds.), *GEOSUR International Symposium on the Geology and Geophysics of the Southernmost Andes, the Scotia Arc and the Antarctic Peninsula*. *Bolletino di Geofisica Teorica ed Applicata*, vol. 45, pp. 15–18.
- Calderón, M., Hervé, F., Massonne, H.-J., Tassinari, C., Pankhurst, R.J., Godoy, E., Theye, T., 2007. *Petrogenesis of the Puerto Edén Igneous and Metamorphic Complex, Magallanes, Chile: Late Jurassic syn-deformational anatexis of metapelites and granitoid magma genesis*. *Lithos* 93, 17–38.
- Casanova, P., 2005. *Estudio sedimentológico de los principales reservorios de la Formación El Salto, en el área de Dorado Sur, Magallanes, Chile*. Graduation Thesis, Universidad de Chile.
- Cox, K.G., Bell, J.D., Pankhurst, R.J., 1979. *The Interpretation of Igneous Rocks*. George, Allen and Unwin Ltd., London.
- Dalziel, I.W.D., 1981. Back-arc extension in the Southern Andes: a review and critical reappraisal. *Philosophical Transactions of the Royal Society of London*. A 300, 319–335.
- Dalziel, I.W.D., Cortés, R., 1972. Tectonic style of the southernmost Andes and the Antarcticandes. XXIV International Geological Congress Section, vol. 3, pp. 316–327.
- Dalziel, I.W.D., de Wit, M.J., Palmer, K.F., 1974. Fossil marginal basin in the southern Andes. *Nature*, London 250, 291–294.
- De la Roche, H., Leterrier, J., Grandclaude, P., Marchal, M., 1980. A classification Of volcanic and plutonic rocks using R1R2-diagram and major element analyses—its relation with current nomenclature. *Chemical Geology* 29, 183–210.
- DePaolo, D.J., Linn, A.M., Schubert, G., 1997. The continental crust age distribution; methods of determining mantle separation ages from Sm–Nd isotopic data and application to the Southwestern United States. *Journal of Geophysical Research* B96, 2071–2088.
- Dzogolyk, E., Hervé, F., Belmar, M., 2003. *Termobarometría de Al en Hornblenda en el Batolito Sur patagónico, entre los 50 y los 52 Latitud sur*. X Congreso Geológico Chileno. CD ROM.
- Eggs, S.M., 2003. Laser ablation ICP-MS analysis of geological materials prepared as lithium borate glasses. *Journal of Geostandards and Geoanalysis* 27, 147–162.
- Eggs, S.M., Kinsley, L.K., Shelley, J.M.G., 1998a. Deposition and element fractionation processes occurring during atmospheric pressure laser sampling for analysis by ICPMS. *Applied Surface Science* 127–129, 278–286.
- Eggs, S.M., Rudnick, R.L., McDonough, W.F., 1998b. The compositions of peridotites and their minerals: a laser-ablation ICP-MS study. *Earth and Planetary Science Letters* 154, 53–71.
- Fanning, C.M., Hervé, F., Pankhurst, R.J., Thomson, S., Faúndez, V., 2001. Late Cenozoic magmatism in the South Patagonian Batholith: Shrimp U–Pb zircon age evidence. III South American Symposium on Isotope Geology, pp. 30–33. CD ROM.
- Féraud, G., Alric, V., Fornari, M., Bertrand, H., Haller, M., 1999. <sup>40</sup>Ar/<sup>39</sup>Ar dating of the Jurassic volcanic province of Patagonia: migrating magmatism related to Gondwana break-up and subduction. *Earth and Planetary Science Letters* 172, 83–96.
- Fildani, A., Cope, T.D., Graham, S.A., Wooden, J.L., 2003. Initiation of the Magallanes foreland basin: timing of the southernmost Patagonian Andes orogeny revised by detrital zircon provenance analysis. *Geology* 31 (12), 1081–1084.
- Forsythe, R., Mpodozis, C., 1983. *Geología del basamento pre-Jurásico Superior en el Archipiélago Madre de Dios, Magallanes, Chile*. Boletín Servicio Nacional de Geología y Minería, vol. 39, 63 pp. Santiago.
- Fuenzalida, R., Covacevich, V., 1988. *Volcanismo y bioestratigrafía del Jurásico y Cretácico Inferior en la Cordillera Patagónica, Región de Magallanes, Chile*. V Congreso Geológico Chileno, pp. H159–H183.
- Glazner, A.F., Bartley, J.M., Coleman, D.S., Gray, W., Taylor, R.Z., 2004. Are plutons assembled over millions of years by

- amalgamation from small magma chambers? *Geological Society of America Today* 14 (4/5), 4–11.
- Govindaraju, K., 1994. Compilation of working values and sample description for 383 geostandards. *Geostandards Newsletter* 18, 1–158.
- Gradstein, F.M., Ogg, J.G., Smith, A.G., Bleeker, W., Lourens, L.J., 2004. A new geologic time scale with special reference to Precambrian and Neogene. *Episodes* 27, 83–100.
- Gust, D.A., Biddle, K.T., Phelps, D.W., Uliana, M.A., 1985. Associated Middle to Late Jurassic volcanism and extension in southern South America. *Tectonophysics* 116, 223–253.
- Halpern, M., 1973. Regional Geochronology of Chile south of 50° latitude. *Geological Society of America Bulletin* 84, 2407–2422.
- Harambour, S., 2002. Deep Seated Thrusts in the Frontal Part of the Magallanes Fold and Thrust Belt, Ultima Esperanza, Chile. XV Congreso Geológico Argentino. CD ROM.
- Hervé, F., Fanning, C.M., 2003. Early Cretaceous subduction of continental crust at the Diego de Almagro archipelago, southern Chile. *Episodes* 26 (4), 285–289.
- Hervé, F., Nelson, E., Kawashita, K., Suarez, M., 1981. New isotopic ages and the timing of orogenic events in the Cordillera Darwin, southernmost Chilean Andes. *Earth and Planetary Science Letters* 55, 257–265.
- Hervé, M., Suárez, M., Puig, A., 1984. The Patagonian batholith south of Tierra del Fuego, Chile: timing and tectonic implications. *Journal of the Geological Society, London* 141, 909–917.
- Hervé, F., Pankhurst, R.J., Trouw, R., Fanning, C.M., Dzogylyk, E., Solari, M., Suárez, M., 2003. Geological Observations at the Western Portion of the Scotia–South America plate Boundary: results of the “Penguin” 2003 Cruise. X Congreso Geológico Chileno. CD ROM.
- Hervé, F., Godoy, E., Mpodozis, C., Fanning, M., 2004. Monitoring magmatism of the Patagonian Batholith through the U–Pb SHRIMP dating of detrital zircons in sedimentary units of the Magallanes Basin. In: Carcione, F., Donda, F., Lodolo, E. (Eds.), *GEOSUR International Symposium on the Geology and Geophysics of the Southernmost Andes, the Scotia Arc and the Antarctic Peninsula*. *Bolletino di Geofisica Teorica ed Applicata*, vol. 45, pp. 113–117.
- Katz, H.R., 1964. Some new concepts on geosynclinal development and mountain building at the southern end of South America. XXII International Geological Congress, India, Proceedings, New Delhi, vol. 4, pp. 242–245.
- Leat, P.T., Scarrow, J.H., Millar, I.L., 1995. On the Antarctic Peninsula batholith. *Geological Magazine* 132, 399–412.
- Longerich, H.P., Jackson, S.E., Günther, D., 1996. Laser ablation inductively coupled plasma mass spectrometric transient signal data acquisition and analyte concentration calculation. *Journal of Analytical Atomic Spectrometry* 11, 899–904.
- Ludwig, K., 1999. *Isoplot/ex, A Geochronological Toolkit for Microsoft Excel*. Special Publication, Berkeley Geochronological Center, vol. 1.
- Martin, M., Pankhurst, R.J., Fanning, C.M., Thomson, S.N., Calderón, M., Hervé, F., 2001. Age distribution of plutons across the Southern Patagonian Batholith: new U–Pb data on zircons. III South American Symposium on Isotope Geology, pp. 585–588. CD ROM.
- Massonne, H.-J., Hervé, F., Calderón, M., Theye, T., 2004. Magmatic muscovite and garnet in granites of the South Patagonian Batholith. In: Carcione, F., Donda, F., Lodolo, E. (Eds.), *GEOSUR International Symposium on the Geology and Geophysics of the Southernmost Andes, the Scotia Arc and the Antarctic Peninsula*. *Bolletino di Geofisica Teorica ed Applicata*, vol. 45, pp. 121–125.
- Michael, P.J., 1991. Intrusion of basaltic magmas into a crystallizing granitic magma chamber; the Cordillera del Paine Pluton in southern Chile. *Contributions to Mineralogy and Petrology* 108, 396–418.
- Mukasa, S., Dalziel, I.W.D., 1996. Southernmost Andes and South Georgia Island, North Scotia Ridge: zircon U–Pb and muscovite Ar–Ar age constraints on tectonic evolution of southwestern Gondwanaland. *Journal of South American Earth Sciences* 9, 349–365.
- Olivares, B., Cembrano, J., Hervé, F., López, G., Prior, D., 2003. Análisis estructural de rocas de una zona de cizalla dúctil en Isla Diego de Almagro, sur de Chile. *Revista Geológica de Chile* 30 (1), 39–52.
- Pankhurst, R.J., Rapela, C.W., 1995. Production of Jurassic rhyolite by anatexis in the lower crust of Patagonia. *Earth and Planetary Science Letters* 134, 23–36.
- Pankhurst, R.J., Weaver, S.D., Hervé, F., Larrondo, P., 1999. Mesozoic–Cenozoic evolution of the North Patagonian Batholith in Aysén, southern Chile. *Journal of the Geological Society, London* 156, 673–694.
- Pankhurst, R.J., Riley, T.R., Fanning, C.M., Kelley, S.P., 2000. Episodic silicic volcanism in Patagonia and the Antarctic Peninsula: chronology of magmatism associated with the break-up of Gondwana. *Journal of Petrology* 41, 603–625.
- Parada, M.A., Lahsen, A., Palacios, C., 1997. Jurassic extensional tectonomagmatism and associated mineralization of the El Faldeo polymetallic district, Chilean Patagonia (Aysén region): geochronological and isotopic evidence of crustal contribution. *Mineralium Deposita* 32, 547–554.
- Pardo-Casas, F., Molnar, P., 1987. Relative motions of the Nazca (Farallon) and South American plates since Late Cretaceous times. *Tectonics* 6, 233–248.
- Pearce, J.A., Harris, N.B.W., Tindle, A.G., 1984. Trace element discrimination diagrams for the tectonic interpretation of granitic rocks. *Journal of Petrology* 25, 956–983.
- Prieto, X., 1987. *Geología regional del sector comprendido entre Seno Ultima Esperanza y Seno Obstrucción: precordillera de la Región de Magallanes*. Graduation Thesis, Universidad de Chile.
- Rapalini, A.E., Hervé, F., Ramos, V.A., Singer, S., 2001. Paleomagnetic evidence for a very large counterclockwise rotation of the Madre de Dios Archipelago, Southern Chile. *Earth and Planetary Science Letters* 184 (2), 471–487.
- Rapela, C.W., Pankhurst, R.J., Fanning, C.M., Hervé, F., 2005. Pacific subduction coeval with the Karoo mantle plume: the Early Jurassic Subcordilleran belt of northwestern Patagonia. In: Vaughan, A.P.M., Leat, P.T., Pankhurst, R.J. (Eds.), *Terrane Accretion Processes at the Pacific Margin of Gondwana*. Special Publication, Geological Society, London, vol. 246, pp. 217–240.
- Riley, T.R., Leat, P.T., Pankhurst, R.J., Harris, C., 2001. Origins of large-volume rhyolite volcanism in the Antarctic Peninsula and Patagonia by crustal melting. *Journal of Petrology* 42, 1043–1065.
- Sánchez, A., Saint Blanquat, M., Hervé, F., Pankhurst, R.J., Fanning, C.M., 2006. A SHRIMP U–Pb zircon Late Miocene crystallization age for the Torres del Paine pluton, Chile. V South American Symposium on Isotope Geology, Short Papers, 196–199, Punta del Este, Uruguay.
- Somoza, R., 1998. Updated Nazca (Farallon)–South America relative motions during the last 40 my: implications for mountain building in the central Andean region. *Journal of South American Earth Sciences* 11, 211–215.
- Stern, C.R., Stroup, J.B., 1982. The petrochemistry of the Patagonian Batholith, Ultima Esperanza, Chile. In: Craddock, C. (Ed.),

- Antarctic Geoscience. University of Wisconsin Press, Madison, pp. 135–142.
- Stern, C.R., de Wit, M.J., 2003. Rocas Verdes ophiolites, southernmost South America: remnants of progressive stages of development on oceanic-type crust in a continental margin back-arc basin. In: Dilek, Y., Robinson, P.T. (Eds.), *Ophiolites in Earth History*. Geological Society London, Special Publications, vol. 218, pp. 1–19.
- Stern, C.R., Mohseni, P.P., Fuenzalida, R., 1991. Petrochemistry and tectonic significance of Lower Cretaceous Barros Arana Formation basalts, southernmost Chilean Andes. *Journal of South American Earth Sciences* 4, 331–342.
- Streckeisen, A., 1976. To each plutonic rock its proper name. *Earth Science Review* 12, 1–33.
- Suárez, M., Hervé, M., Puig, A., 1986. K–Ar dates on granitoids from Archipelago Cabo de Hornos, southernmost Chile. *Geological Magazine* 123 (5), 581–584.
- Suárez, M., Hervé, M., Puig, A., 1987. Cretaceous diapiric plutonism in the southern Cordillera, Chile. *Geological Magazine* 124 (6), 569–575.
- Sun, S.S., McDonough, W.F., 1989. Chemical and isotopic systematics of oceanic basalts: implications for mantle compositions and processes. In: Saunders, A.D., Norry, M.J. (Eds.), *Magmatism in Ocean Basins*. Special Publication, Geological Society, London, vol. 42, pp. 313–345.
- Thomson, S.N., Hervé, F., 2002. New time constraints for the age of metamorphism at the ancestral Pacific Gondwana margin of southern Chile. *Revista Geológica de Chile* 29 (2), 255–271.
- Thomson, S.N., Hervé, F., Stöckert, B., 2001. Mesozoic–Cenozoic denudation history of the Patagonian Andes (southern Chile) and its correlation to different subduction processes. *Tectonics* 20, 693–711.
- Ureta, M., 2000. Estudio petrológico del Batolito Surpatagónico entre los 48° y 51° L.S. Graduation Thesis, Departamento de Geología, Universidad de Chile.
- Weaver, S.G., Bruce, R., Nelson, E.P., Brueckner, H.K., LeHuray, A.P., 1990. The Patagonian Batholith at 48°S latitude, Chile: geochemical and isotopic variations. In: Kay, S.M., Rapela, C.W. (Eds.), *Plutonism from Alaska to Antarctica*. Special Paper, Geological Society of America, vol. 241, pp. 33–50.
- Wigger, P.J., Schmitz, M., Araneda, M., Asch, G., Baldzuhn, S., Giese, P., Heinsohn, W.D., Martínez, E., Ricaldi, E., Röwer, P., Viramonte, J., 1994. Variation in the crustal structure of the Southern Central Andes deduced from seismic refraction investigations. In: Reutter, K.-J., Sheuber, E., Wigger, P.J. (Eds.), *Tectonics of the Southern Central Andes*. Springer, Berlin, pp. 23–48.
- Williams, I.S., 1998. U–Th–Pb geochronology by ion microprobe. In: McKibben, M.A., Shanks III, W.C., Ridley, W.I. (Eds.), *Applications of microanalytical techniques to understanding mineralizing processes*. *Reviews in Economic Geology*, vol. 7, pp. 1–35.
- Willner, A.P., Hervé, F., Thomson, S.N., Massonne, H.-J., 2004. Converging P–T paths of Mesozoic HT–LT metamorphic units (Diego de Almagro Island, Southern Chile): evidence for juxtaposition during late shortening of an active continental margin. *Mineralogy and Petrology* 41, 43–84.
- Yuan, X., Sobolev, S.V., Kind, R., Oncken, O., Bock, G., Asch, G., Schurr, B., Graeber, F., Rudloff, A., Hanka, W., Wylegalla, K., Tibi, R., Haberland, C., Rietbrock, A., Giese, P., Wigger, P., Rower, P., Zandt, G., Beck, S., Wallace, T., Pardo, M., Comte, D., 2000. Subduction and collision processes in the Central Andes constrained by converted seismic phases. *Nature* 408, 958–961.